The Astrophysical Journal Supplement Series, 223:6 (20pp), 2016 March doi:10.3847/0067-0049/223/1/6

KINEMATIC DISTANCES OF GALACTIC PLANETARY NEBULAE

A. Y. Yang[1,2], W. W. Tian[1,2,3], H. Zhu[1,2], D. A. Leahy[3], and D. Wu[1,4,5]
[1] Key Laboratory of Optical Astronomy, National Astronomical Observatories, Chinese Academy of Sciences, Beijing 100012, China; tww@bao.ac.cn, ayyang@bao.ac.cn
[2] University of Chinese Academy of Science, 19A Yuquan Road, Beijing 100049, China
[3] Department of Physics & Astronomy, University of Calgary, Calgary, Alberta T2N 1N4, Canada
[4] College of Information Science and Technology, Beijing Normal University, Beijing 100875, China
[5] Beijing Key Laboratory of Digital Preservation and Virtual Reality for Cultural Heritage, Beijing 100875, China
Received 2015 November 10; accepted 2016 January 15; published 2016 March 23

ABSTRACT

We construct H I absorption spectra for 18 planetary nebulae (PNs) and their background sources using data from the International Galactic Plane Survey. We estimate the kinematic distances of these PNs, among which 15 objects' kinematic distances are obtained for the first time. The distance uncertainties of 13 PNs range from 10% to 50%, which is a significant improvement with uncertainties of a factor of two or three smaller than most previous distance measurements. We confirm that PN G030.2−00.1 is not a PN because of its large distance found here.

Key words: ISM: clouds – ISM: kinematics and dynamics – planetary nebulae: general – stars: distances

1. INTRODUCTION

Distances, as a basic physical parameter of planetary nebulae (PNs), are crucial for studying their size, luminosity, ionized mass, formation rate, space density, and Galactic distribution. However, distances are still not well determined for the majority of a total of ~3500 PNs (Kwitter et al. 2014). For an individual PN, different methods may lead to different distances. So far, there are only about 30 PNs with distance measurements with uncertainties less than 20%.

Nine popular methods have been used to measure the distances of PNs, including trigonometric parallax (e.g., Harris et al. 2007), cluster member (e.g., Jacoby et al. 1997), expansion parallax (e.g., Terzian 1997), spectroscopic parallax (e.g., Ciardullo et al. 1999), reddening (e.g., Gathier et al. 1986b), Na D absorption (e.g., Napiwotzki & Schoenberner 1995), determinations of central star gravities (e.g., Mendez et al. 1988), a statistical method (revised Shklovsky method, e.g., Cahn et al. 1992), and a kinematics method (e.g., Gathier et al. 1986a).

Hydrogen is the most abundant element in the universe and H I atom clouds are broadly distributed in the Milky Way (Dickey & Lockman 1990). The 21 cm H I absorption line has been widely used to measure kinematic distances of H I clouds and associated strong radio sources. When an H I cloud is located in front of or behind a strong radio source, we are usually able to detect an H I absorption feature or only an emission line from the cloud. The velocity of the emission/absorption feature can be converted into a distance based on the axisymmetric rotation curve model for the Galaxy. The distance or distance limit of the source can be estimated from the distance of the H I cloud. However, this method faces two main challenges. One is the kinematic distance ambiguity (KDA) for sources located inside the solar circle, as each radial velocity along a given line of sight corresponds to two distances equally spaced on either side of the tangent point. The KDA can usually be solved by the integrated consideration of H I absorption/self-absorption, CO emission, and H I absorption of background sources. Another challenge is to construct a reliable H I absorption spectrum to a radio source due to the uneven H I background in the Galaxy. In order to minimize the second effect, Tian et al. (2007) and Leahy & Tian (2008) developed revised methods to construct H I absorption spectra. The methods have been applied to several types of Galactic objects successfully, e.g., PNs (Zhu et al. 2013), supernova remnants, and H II regions (e.g., Leahy & Tian 2008; Tian & Leahy 2008).

In this paper, we systematically construct the H I absorption spectra of PNs which are located in the sky region of the International Galactic Plane Survey (IGPS). H I absorption features in the spectra are used to determine the distances of the PNs. This paper is organized as follows: the data and the revised methods are introduced in Section 2. In Section 3, we apply the methods to estimate individual PN distances. A summary is given in Section 4.

2. DATA ANALYSIS

2.1. Data

The 1420 MHz radio continuum and H I line emission data come from IGPS (the Very Large Array Galactic Plane Survey (Stil et al. 2006), the Southern Galactic Plane Survey (SGPS; McClure-Griffiths et al. 2005), and the Canadian Galactic Plane Survey (CGPS; Taylor et al. 2003)). The project surveys the Galactic disk from longitudes 18°–67°, 255°–357°, and 65°–175°, respectively. For CGPS, the continuum image at 1420 MHz has a spacial resolution of $1'$ and H I spectra line images have resolutions of $1' \times 1' \times 1.56$ km s^{-1}. At declination δ, the synthesized beam is $49'' \times 49'' csc\delta$ for 1420 MHz and $58'' \times 58'' csc\delta \times 1.32$ km s^{-1} for H I in the survey of CGPS. SGPS has a resolution $100''$ for continuum and $\sim 2' \times 2' \times 1$ km s^{-1} for H I data. The ^{13}CO spectral line data from the Galactic Ring Survey of the Five College Radio Astronomical Observatory (FCRAO) 14 m telescope (Jackson et al. 2006) has an angular and spectral resolution of $46''$ and 0.21 km s^{-1} at longitudes from 18° to 52° and latitudes between −1° and 1°. The ^{12}CO (J = 1−0) spectral line data from the FCRAO CO Survey of the Outer Galaxy has an angular and spectral resolution of $45''$ and 0.98 km s^{-1} between Galactic longitudes 102°.49–141°.54 and latitudes −3°.03–5°.41 (Heyer & Terebey 1998).

In this work, we construct the H I absorption spectra of the PNs with flux density larger than 50 mJy at 1420 MHz in the

Table 1
Information on PNs and Background Sources

PN G Name	l (°)	b (°)	$S_{1.4\mathrm{GHz}}$ (mJy)	Survey	Ref.	Background l	Sources b
G020.9−01.1	20.999	−1.125	249.0 ± 7.5	V	CK98	21.345	−0.630
						21.500	−0.885
G029.0+00.4	29.079	0.454	159.0 ± 15	V	CK98	28.800	0.175
						28.825	−0.230
						29.098	0.545
G030.2−00.1	30.234	−0.139	…[a]	V	A11	29.930	−0.055
						30.535	0.020
						30.685	−0.260
						29.960	−0.020
G051.5+00.2	51.509	0.167	84.0	V	LCY05	51.775	0.800
						50.625	−0.030
						50.950	0.850
G052.1+01.0	52.099	1.043	455.1 ± 13.7	V	IPHAS09	52.235	0.745
						52.750	0.335
G055.5 − 00.5	55.507	−0.558	84.1 ± 2.6	V	CK98	55.525	−1.150
						55.995	−1.195
						55.775	−0.250
G069.7−00.0	69.800	0.004	87.1 ± 2.6	V	CK98	68.755	0.275
						70.155	0.090
G070.7+01.2	70.674	1.192	949.6 ± 33.4	C	IPHAS09	71.225	1.445
						70.690	0.630
						70.600	1.380
G084.9−03.4	84.930	−3.496	1373 ± 41	C	CK98	85.120	−3.100
						84.445	−2.915
G089.0+00.3	89.002	0.376	260.5 ± 7.8	C	IPHAS09	88.825	0.925
						88.465	0.004
						89.650	0.925
G107.8+02.3	107.845	2.314	581 ± 22.8	C	IPHAS09	108.755	2.575
G138.8+02.8	38.816	2.805	153.1 ± 5.8	C	CK98	138.795	2.140
G147.4−02.3	147.401	−2.307	77.8 ± 2.4	C	IPHAS09	146.625	−2.690
						147.950	−2.645
G169.7−00.1	169.653	−0.077	135.3 ± 5.1	C	IPHAS09	169.080	−0.245
						170.330	−0.225
G259.1+00.9	259.149	0.940	345 ± 12	S	CK98	257.902	0.844
						257.913	0.655
G333.9+00.6	333.930	0.686	294.8 ± 9.7	S	BPF11	333.723	0.377
						332.967	0.777
G352.6+00.1	352.675	0.144	378 ± 38	S	CK98	352.588	−0.167
						351.616	0.177
						353.408	−0.355
G352.8 − 00.2	352.828	−0.259	474 ± 47	S	CK98	352.588	−0.167
						352.854	−0.189
						353.408	−0.355

Note. The first three columns give the name and Galactic coordinates. Column (4) gives the flux density at 1.4 GHz. The survey names and references are given in the next two columns. The final two columns give the Galactic coordinates of background sources. References given in the table are as follows: IPHAS09, Viironen et al. (2009); CK98, Condon & Kaplan (1998); LCY05, Luo et al. (2005); BPF11, Bojičić et al. (2011); A11, Anderson et al. (2011).
[a] T he flux at 8.7 GHz is 752 mJy for PN G030.2−00.1.

IGPS. By checking their H I spectra visually individually, 18 of them show reliable absorption features. We analyze the 18 PNs in this paper. For each PN, at least one bright nearby background source has been chosen as a comparison with the PN in order to understand the PN's H I absorption spectrum. The parameters of the 18 PNs and their background sources are shown in Table 1.

2.2. To Obtain a Reliable H I Absorption Spectrum

Based on the knowledge of radiation transfer, the brightness temperature of the source (T_{on}) and background (T_{off}) that have continuum emission subtracted can be determined by the equations:

$$T_{\mathrm{on}}(\nu) = T_{\mathrm{B}}(\nu)(1 - e^{-\tau(\nu)}) + T_{\mathrm{S}}^{\mathrm{C}}(e^{-\tau_{\mathrm{c}}(\nu)} - 1) \tag{1}$$

$$T_{\mathrm{off}}(\nu) = T_{\mathrm{B}}(\nu)(1 - e^{-\tau(\nu)}) + T_{\mathrm{bg}}^{\mathrm{C}}(e^{-\tau_{\mathrm{c}}(\nu)} - 1). \tag{2}$$

So, we can obtain the absorption spectrum of H I,

$$e^{-\tau_{\mathrm{c}}(\nu)} = 1 - \frac{T_{\mathrm{off}}(\nu) - T_{\mathrm{on}}(\nu)}{T_{\mathrm{S}}^{\mathrm{C}} - T_{\mathrm{bg}}^{\mathrm{C}}}, \tag{3}$$

Where $T_{\mathrm{B}}(\nu)$ is the spin temperature of the H I cloud, and $T_{\mathrm{S}}^{\mathrm{C}}$ and $T_{\mathrm{bg}}^{\mathrm{C}}$ are the continuum brightness temperatures of

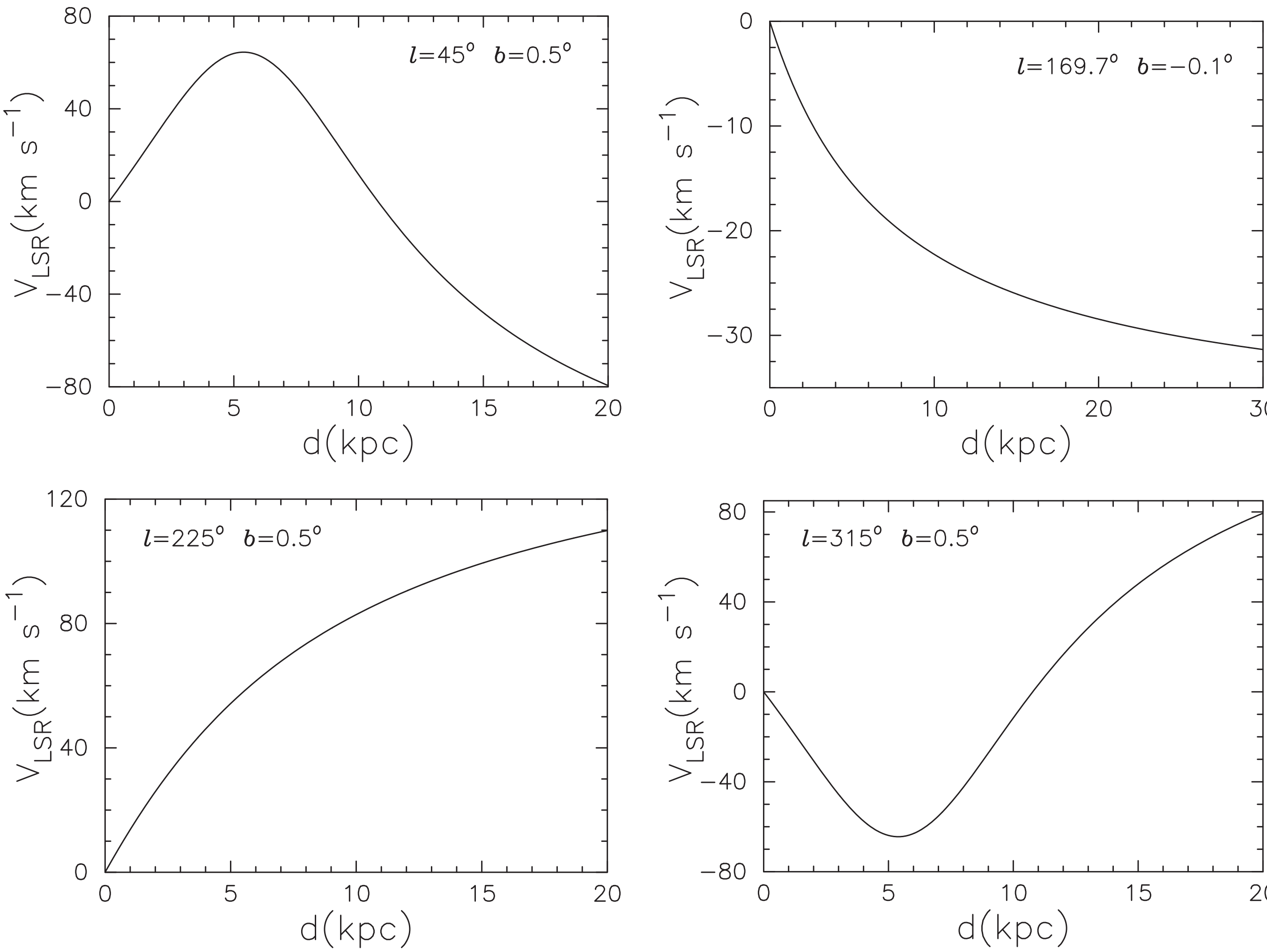

Figure 1. Relation between heliocentric distance d and radial velocity V_r in the four quadrants in the direction (l, b) in Galactic coordinates, using a Galactic circular rotation curve model and adopting a galactocentric distance of $R_0 = 7.62$ kpc and a rotation velocity of $V_0 = 220$ km s^{-1}.

the source and background. The H I absorption spectrum is usually represented by $e^{-\tau_c(\nu)}$, or sometimes by τ_c.

To construct a H I absorption spectrum, traditionally one usually chooses the source and background regions separately. This could increase the possibility of a false absorption spectrum caused by the different distributions of H I clouds along the two lines of sight. Nevertheless, Tian et al. (2007) and Leahy & Tian (2008) proposed revised methods by selecting the background region directly surrounding the source region to minimize the possibility of a false H I absorption spectrum. In addition, they extracted the CO emission spectrum in the source direction and constructed the H I absorption spectra of nearby strong background sources with angular separations not exceeding 1° from target source to better understand the target source's absorption spectrum. Additionally, when possible, H I self-absorption resulting from the cold H I cloud absorbing emission from the background warm H I cloud at the same velocity has been used to reduce the KDA problem in the methods (e.g., Leahy & Tian 2010; Tian et al. 2010).

3. KINEMATIC DISTANCE MEASUREMENT TO PNS

3.1. The Model

The methods of determining distances are based on the flat Galactic circular rotation curve model. For a given PN at a distance d from the Sun in the direction of (l, b) in Galactic coordinates, the relation between the heliocentric distance d and the galactocentric distance R can be written as

$$R^2 = R_0^2 + d^2\cos^2 b - 2R_0 d\cos b\cos l, \tag{4}$$

where $R_0 = 7.62 \pm 0.32$ kpc (Eisenhauer et al. 2005), the distance to the Galactic center from the Sun. However, R_0 is still uncertain (e.g., Bovy et al. 2012). Assuming circular orbits, the rotation velocity V_R at galactocentric distance R is given by

$$V_R = \frac{R}{R_0}\left(\frac{V_r}{\cos b\sin l} + V_0\right), \tag{5}$$

where V_r is the radial velocity corresponding to the local standard of rest (LSR), and $V_0 = 220$ km s^{-1} is the IAU adopted velocity at the LSR. In this work, we focus on the relation between the heliocentric distance d and the radial velocity V_r. Since d can be expressed by

$$d = \frac{R_0\cos l \pm \sqrt{R^2 - (R_0\sin l)^2}}{\cos b}, \tag{6}$$

where R is related to V_r in Equation (5), the heliocentric distance d can be written as a function of the radial velocity V_r, which has different forms of expression in the four quadrants of

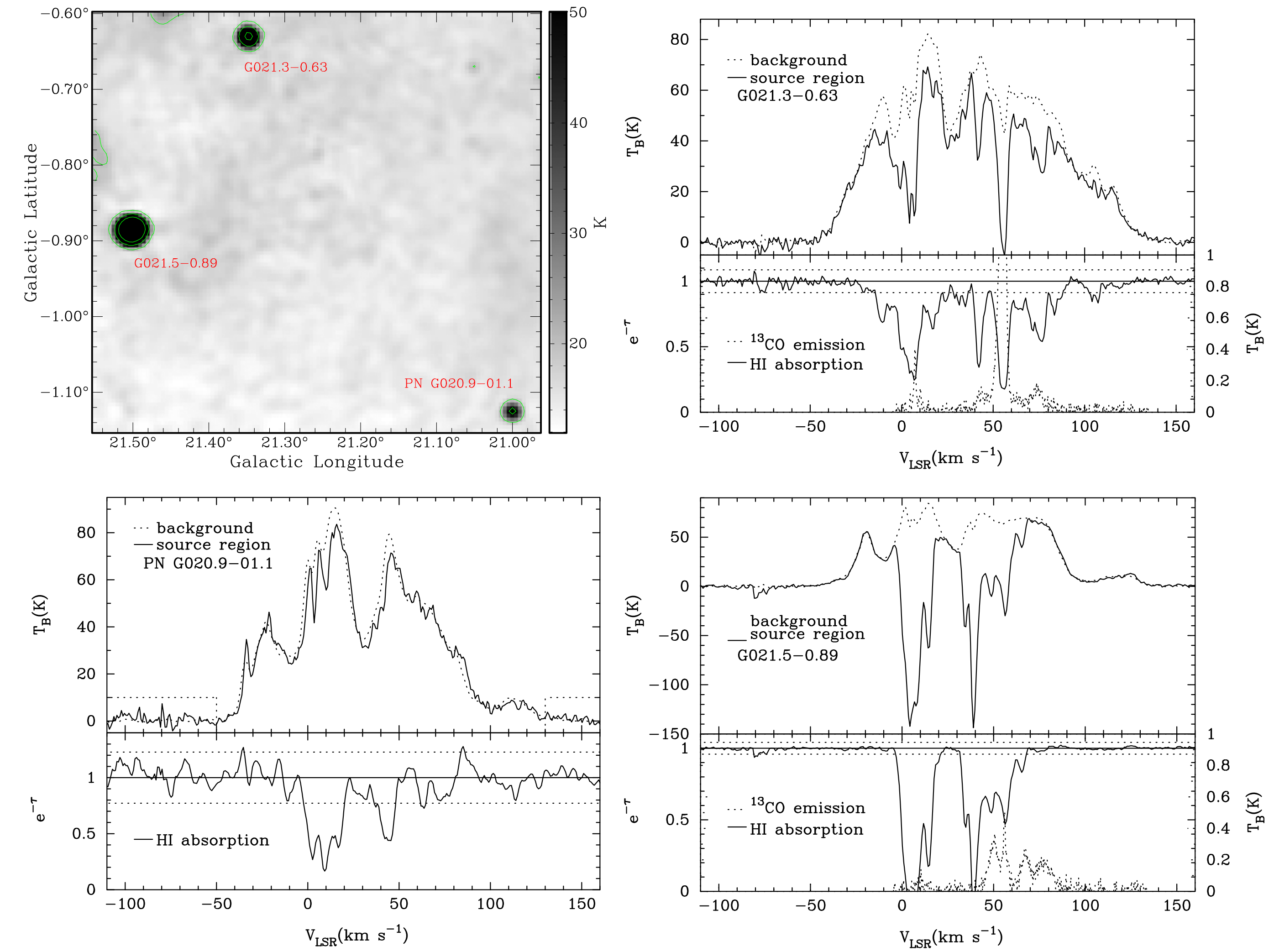

Figure 2. 1420 MHz continuum image of PN G020.9−01.1 and its background sources (top left), and the H i spectra of PN G020.9−01.1 (bottom left), G021.3−0.63 (top right), and G021.5−0.89 (bottom right). The map has superimposed contours (20, 50, 130 K) of 1420 MHz continuum emission. The dotted horizontal lines in the lower panel of the PN spectrum show the 3σ noise level. This description applies for all the spectra of PNs and background sources from Figures 2–19.

the Galactic coordinates; see Figure 1. In general, we analyze the spectra of PNs and their background sources to determine the kinematic distances of PNs assuming $V_R = V_0$. In some special cases, when the maximum observed radial velocity (tangent point velocity) in the PN spectrum is much larger than the expected value, i.e., $V_R > V_0$, we consider V_R linearly increasing from $V_0 = 220\,\mathrm{km\,s^{-1}}$ to V_R as R reduces to the value at the tangent point. The same situation has been discussed in Leahy et al. (2008). We note that Reid et al. (2007) updated the value V_0/R_0 with $V_0 = 224\,\mathrm{km\,s^{-1}}$ and $V_R = 242\,\mathrm{km\,s^{-1}}$. Reid et al. (2009) also found a higher rotation velocity of $V_0 = 254 \pm 16\,\mathrm{km\,s^{-1}}$ by measuring the trigonometric parallaxes and proper motions of masers with the Very Long Baseline Array data. Likewise, Leahy et al. (2008) and Levine et al. (2008) suggested a higher rotation velocity at longitude near 53°.

3.2. Application to PN

We estimate the distances of 18 PNs by taking 3σ as the minimum level of significance for the detection of an H i absorption feature, where σ is the standard deviation calculated from the no emission baseline of the PN H i spectrum. The distance uncertainty includes that caused by an average random velocity of H i clouds, i.e., $\sim 6\,\mathrm{km\,s^{-1}}$ (Crovisier 1978; Shaver et al. 1982; Anantharamaiah et al. 1984). For each PN, at least one bright background source within an angular separation of 1° from the PNs has been chosen. The spectra are used to compare with that of the PN in order to understand the PN's absorption spectrum. The 1420 MHz continuum images of both PNs and background sources are displayed in Figures 2–19, together with their H i absorption spectra. The distance for each individual PN is discussed below, taking $R_0 = 7.62$ kpc.

PN G020.9−01.1 (Figure 2).

Figure 2 shows the 1420 MHz continuum image and H i spectra of PN G020.9−01.1 and its nearby background sources (G021.3−0.63, G021.5−0.89). The PN is fainter in the radio than both G021.3−0.63 and G021.5−0.89 so that the PN H i absorption spectrum shows more noise than the others. The absence of absorption at the tangent point velocity ($\sim 100\,\mathrm{km\,s^{-1}}$) for both PN G020.9−01.1 and G021.5−0.89 implies they are likely located in front of the tangent point (7.1 ± 0.6 kpc). The spectrum of G021.3−0.63 shows absorption features at $105\,\mathrm{km\,s^{-1}}$ and negative velocities,

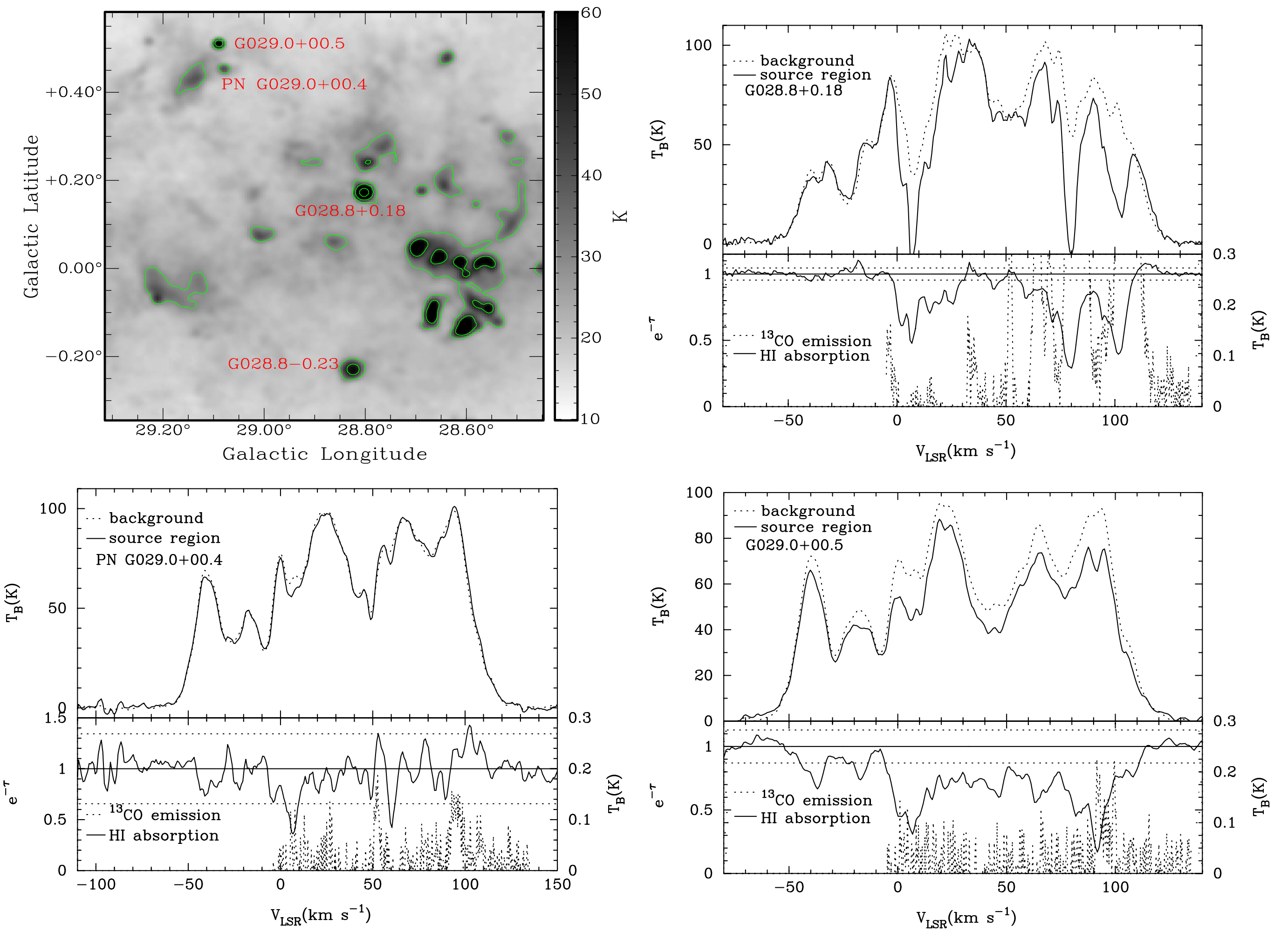

Figure 3. 1420 MHz continuum image of PN G029.0+00.4 and its background sources (top left), and the H i spectra of PN G029.0+00.4 (bottom left), G028.8+0.18 (top right), and G029.0+00.5 (bottom right). The H i spectra of G028.8−0.23 is listed in Figure 21. The map has superimposed contours (30, 50, 120 K) of the 1420 MHz continuum emission.

which supports that this source is further than both PN G020.9 −01.1 and G021.5−0.89. The absorption feature at 62 km s^{-1} is probably not real since the absorption is very close to 3σ. The reliable absorption feature at 45 km s^{-1} ($e^{-\tau} = 0.44$) indicates a lower limit distance of 3.1 ± 0.3 kpc for the PN, i.e., the nearside distance for this velocity.

For PN G020.9−01.1, Cazetta & Maciel (2001) found a distance of 2.4 kpc based on the relation between distance and the surface gravity of the central star of a PN ($d^2 \propto M_\odot F_* g^{-1} 10^{0.4V_0}$). This kinematic distance of 3.1 ± 0.3 kpc is reasonably consistent with the surface gravity distance, and larger than previous statistical distances of 1.75 kpc by Cahn et al. (1992), 1.66 kpc by van de Steene & Zijlstra (1995), 1.74 kpc by Zhang (1995), 2.29 kpc by Stanghellini et al. (2008), and 1.59 kpc by Phillips (2004).

PN G029.0+00.4 (Figure 3).

Although the background sources near PN G029.0+00.4 show clear absorption spectra, the PN spectrum is complex. The prominent emission at the tangent point (∼100 km s^{-1}) and the absence of an absorption feature at the velocity in the PN spectrum indicate an upper limit distance of 6.6 ± 1.0 kpc for the PN. One probable absorption feature at 60 km s^{-1} implies a lower limit distance of 3.5 ± 0.3 kpc.

For this PN, a distance of 1.2 kpc has been derived by Maciel (1984), assuming a relationship between the nebular ionized mass and radius, which is smaller than our result.

PN G030.2−00.1 (Figure 4).

PN G030.2−00.1 is a PN candidate suggested by Anderson et al. (2011). The absorption features of the PN candidate and four H ii regions appear up to the tangent point velocity (∼110 km s^{-1}), which indicates all five objects are beyond the tangent point, i.e., 6.6 ± 0.9 kpc. The absence of absorption at negative velocity in the PN spectrum implies the PN is inside the solar circle (13.2 ± 0.5 kpc). The obvious absorption feature in the PN spectrum and the absence of absorption in the spectra of all background sources at 40 km s^{-1} imply that the PN is likely beyond the far side distance of 40 km s^{-1}, i.e., 10.7 ± 0.3 kpc. Based on this information, the PN sits between 10.7 ± 0.3 kpc and 13.2 ± 0.5 kpc.

PN G051.5+00.2 (Figure 5).

Based on the Galactic circular rotation curve model and the IAU adopted parameters of $V_0 = 220$ km s^{-1}, the tangent velocity $V_\perp$ is expected to be 48 km s^{-1}. This is much smaller than the observed value of $V_\perp \simeq 70$ km s^{-1} obtained from the H i emission spectrum in Figure 5. This higher $V_\perp$ could be due to the spiral arm velocity perturbation near the tangent point in the direction of $l = 51\overset{\circ}{.}5$ (Dobbs et al. 2006). If

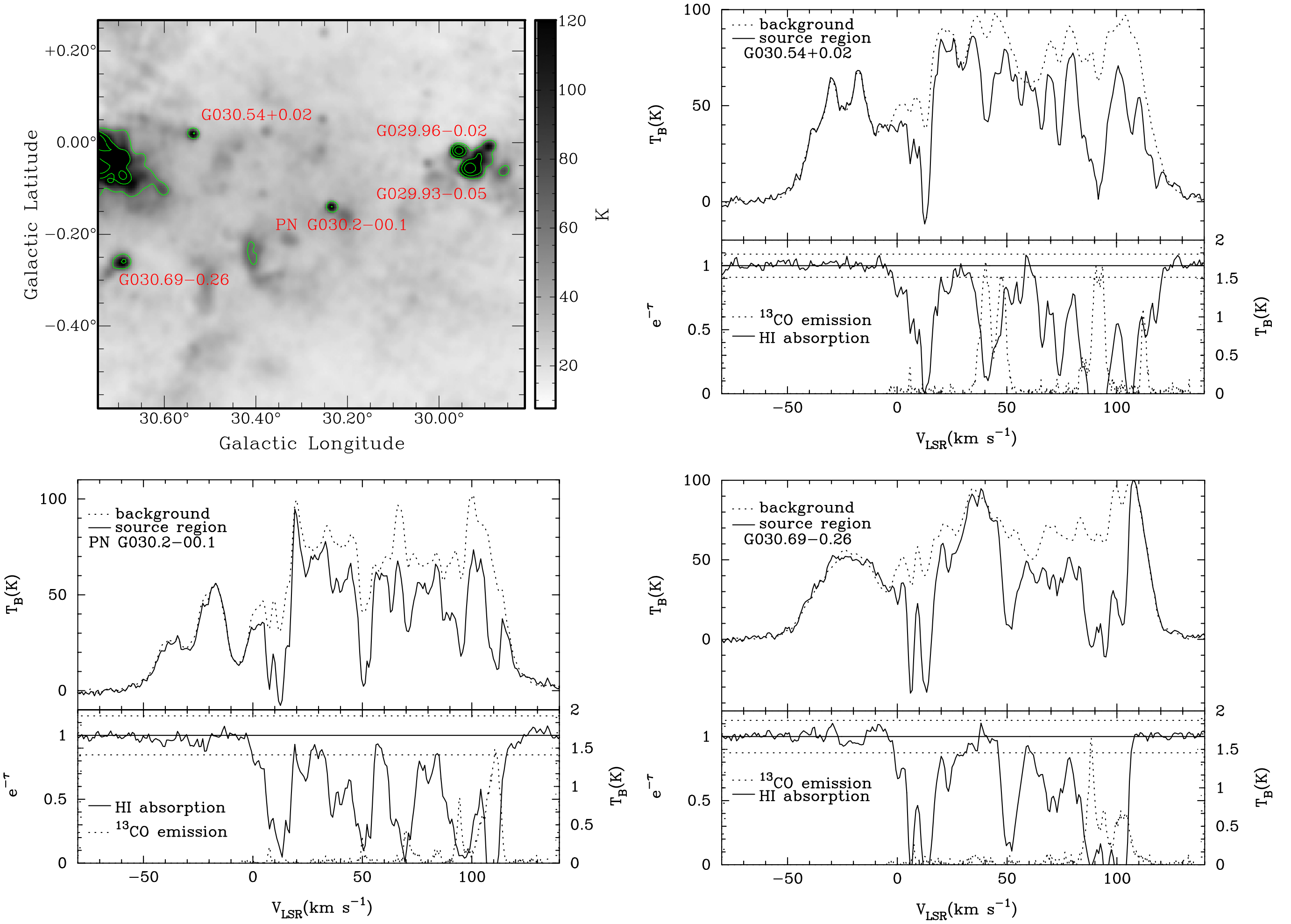

Figure 4. 1420 MHz continuum image of PN G030.2−00.1 and its nearby background source (top left), and the H I spectra of PN G030.2−00.1 (bottom left), G030.54+0.02 (top right), and G030.69−0.26 (bottom right). The H I spectra of G029.93−0.05 and G029.96−0.02 are listed in Figure 21. The map has superimposed contours (65, 125, 230 K) of the 1420 MHz continuum emission.

$V_\perp = 70\,\mathrm{km\,s^{-1}}$, the rotation velocity V_R would be as high as 242 km s^{-1}. In fact, Levine et al. (2008) found a high rotation velocity of ∼236 km s^{-1} at longitudes near 53°. In addition, the high rotation velocity is also obtained in the H I spectra of PN G052.1+01.0 and PN G055.5−00.5. Altogether, we calculate the kinematic distance to the PN using $R_0 = 7.62$ kpc, $V_0 = 220\,\mathrm{km\,s^{-1}}$, and $V_R = 243\,\mathrm{km\,s^{-1}}$.

The PN spectrum reveals that absorptions appear up to the tangent point velocity, giving a lower limit distance of 4.7 ± 1.4 kpc. The absence of any absorption feature at negative velocities in the PN spectrum means that the PN is within the solar circle, giving an upper limit distance of 9.5 ± 0.4 kpc.

PN G052.1+01.0 (Figure 6).

Similar to PN G051.5+00.2, the observed tangent point velocity of 68 km s^{-1} from the PN H I spectrum is larger than the expected value of 46 km s^{-1} when taking commonly used parameters of $V_0 = 220\,\mathrm{km\,s^{-1}}$. This leads to a rotation velocity up to $V_R = 242\,\mathrm{km\,s^{-1}}$. Figure 6 shows absorption features in the spectra of the PN and two H II regions (G052.2+0.75, G052.7+0.3) up to the tangent point velocity (68 km s^{-1}), revealing that all three objects are beyond the tangent point. So the lower limit distance for this PN is 4.7 ± 1.4 kpc. Bright H I emission is detected at 48 km s^{-1} in the three spectra, whereas the absorption feature at this velocity is detected only in the spectra of two H II regions. This implies that the PN is in front of H I at its far side distance of 5.6 ± 0.8 kpc.

PN G055.5−00.5 (Figure 7).

The observed tangent point velocity (55 km s^{-1}) in the PN spectrum is larger than the expected value (38 km s^{-1}), which suggests that the rotation velocity is $V_R = 236\,\mathrm{km\,s^{-1}}$ at the tangent point. Absorption features at the tangent point velocity in the spectra of the PN as well as three background sources (G055.5−01.1, G055.9−01.2, and G055.7−00.2) indicate that all four objects are beyond the tangent point. Therefore, the lower limit distance is 4.3 ± 1.5 kpc for the PN. The absence of absorption in the PN spectrum at negative velocities implies that the PN is within the solar cycle. So we suggest that the distance of the PN is between 4.3 ± 1.5 kpc and 8.6 ± 0.4 kpc.

Giammanco et al. (2011) suggested a distance of 2.9 ± 0.4 based on distance-extinction relationship in the direction toward the PN. Zhang (1995) derived a distance of 3.17 kpc by using the relation between the radio continuum surface brightness and the nebular radius. Stanghellini et al. (2008) obtained a distance of 3.68 kpc by the revised relation of

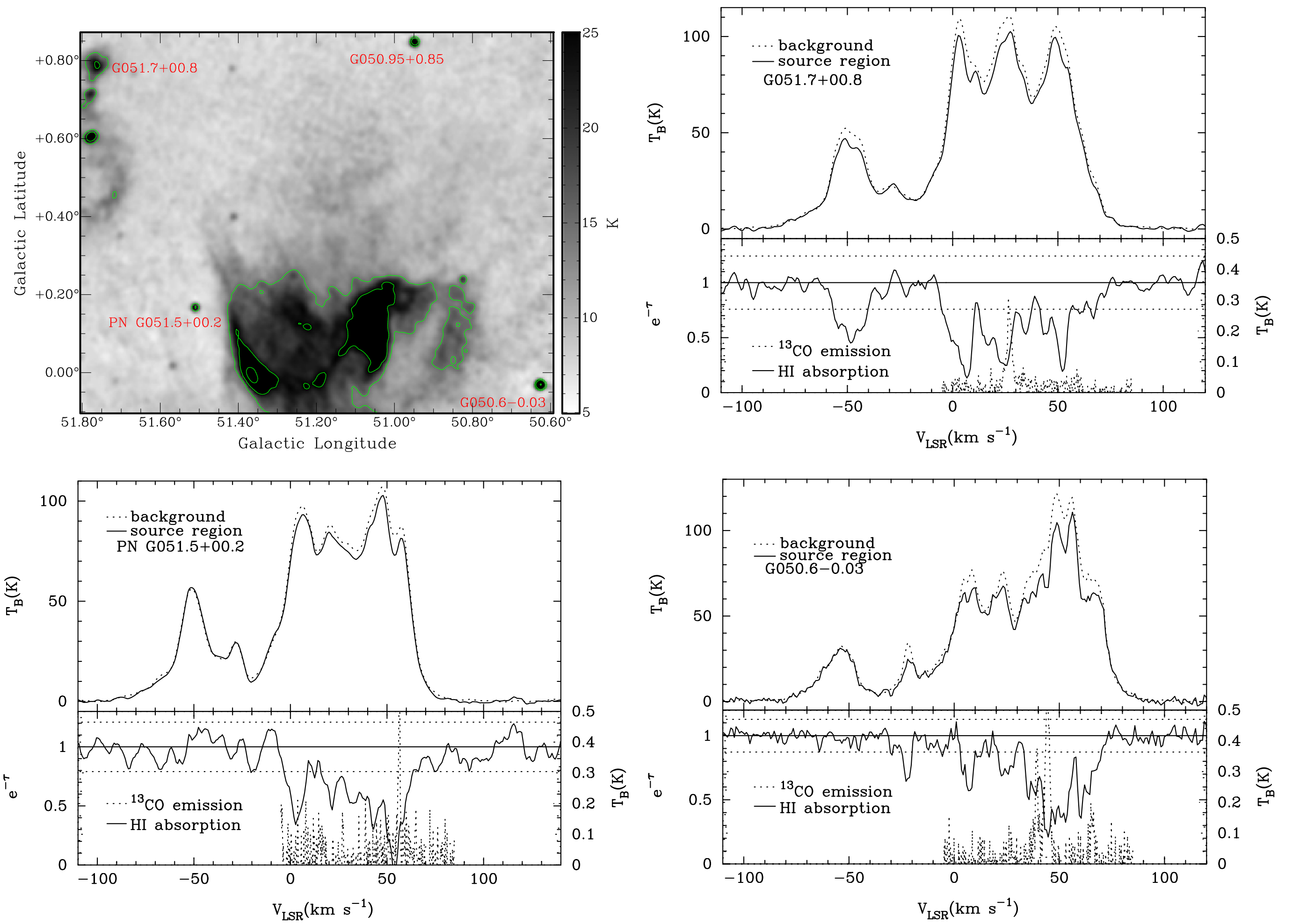

Figure 5. 1420 MHz continuum image of PN G051.5+00.2 and its nearby background sources (top left), and the H I spectra of PN G051.5+00.2 (bottom left), G051.7+00.8 (top right), and G050.6−00.3 (bottom right). The H I spectra of G050.95+0.85 is shown in Figure 21. The map has superimposed contours (15, 25, 60 K) of the 1420 MHz continuum emission.

ionized mass and optical thickness. So our lower limit distance of 4.3 ± 1.5 kpc for the PN G055.5−00.5 is reasonable.

PN G069.7−00.0 (Figure 8).

The PN spectrum has a low signal-to-noise ratio (S/N) due to its low brightness. Significant absorption features are detected at the tangent point velocity and at negative velocities in the spectra of both the PN and its background sources, hinting that they are all beyond the solar circle ($d = 5.3 \pm 0.7$ kpc). According to the noise level ($3\sigma = 0.23$), the H I emission and absorption features at -64 km s^{-1} reveal a lower limit distance of 11.1 ± 0.6 kpc for the PN. The presence of H I emission at -73 km s^{-1} and the absence of an absorption feature at the same velocity indicate an upper limit distance of 12.0 ± 0.7 kpc. In summary, PN G069.7−00.0 has distance between 11.1 ± 0.6 kpc and 12.0 ± 0.7 kpc, which is much larger than previous distances, e.g., 3.31 kpc by (Cahn et al. 1992), 3.26 kpc by Zhang (1995), 4.23 kpc by Stanghellini et al. (2008), 3.09 kpc by van de Steene & Zijlstra (1995), and 2.96 kpc by Phillips (2004). So we prefer to keep its distance as an open question.

PN G070.7+01.2 (Figure 9).

Based on the observed tangent point velocity of 22 km s^{-1} in the PN spectrum, we take a rotational velocity $V_R = 230$ km s^{-1} at the tangent point in the direction $l = 70\overset{\circ}{.}7$. The fact that the H I absorption features of the PN and three background sources appear at the tangent point velocity implies all sources are beyond the tangent point. So we obtain a lower limit distance of 2.5 ± 1.6 kpc for the PN. There are clear absorption features at negative velocities in the spectra of nearby sources, while no absorption feature is detected at these velocities in the PN spectrum. This implies the PN is within the solar circle (5.0 ± 0.7 kpc). So PN G070.7+01.2 is between 2.5 ± 1.6 kpc and 5.0 ± 0.7 kpc.

Bally et al. (1989) have given a distance of 4.5 ± 1.0 kpc using the line width of CO emission and the angular radius of the CO cloud. Therefore, the upper distance of 5.0 ± 0.7 kpc is suitable for the PN.

PN G084.9−03.4 (Figure 10).

Figure 10 shows the tangent point velocity (18 km s^{-1}) toward the PN, which is larger than the expected value (0.8 km s^{-1}). We obtain the rotation velocity $V_R = 237$ km s^{-1} at the tangent point in the direction $l = 84\overset{\circ}{.}9$. The H I spectra of the PN and two background sources show clear H I absorption features from ∼0 km s^{-1} up to the tangent point (18 km s^{-1}), hinting that the PN and two background sources are beyond the tangent point. So we obtain the lower limit distance of ∼0.7 kpc for this PN. The prominent H I emission at -20 km s^{-1} appears in the spectra of the PN as

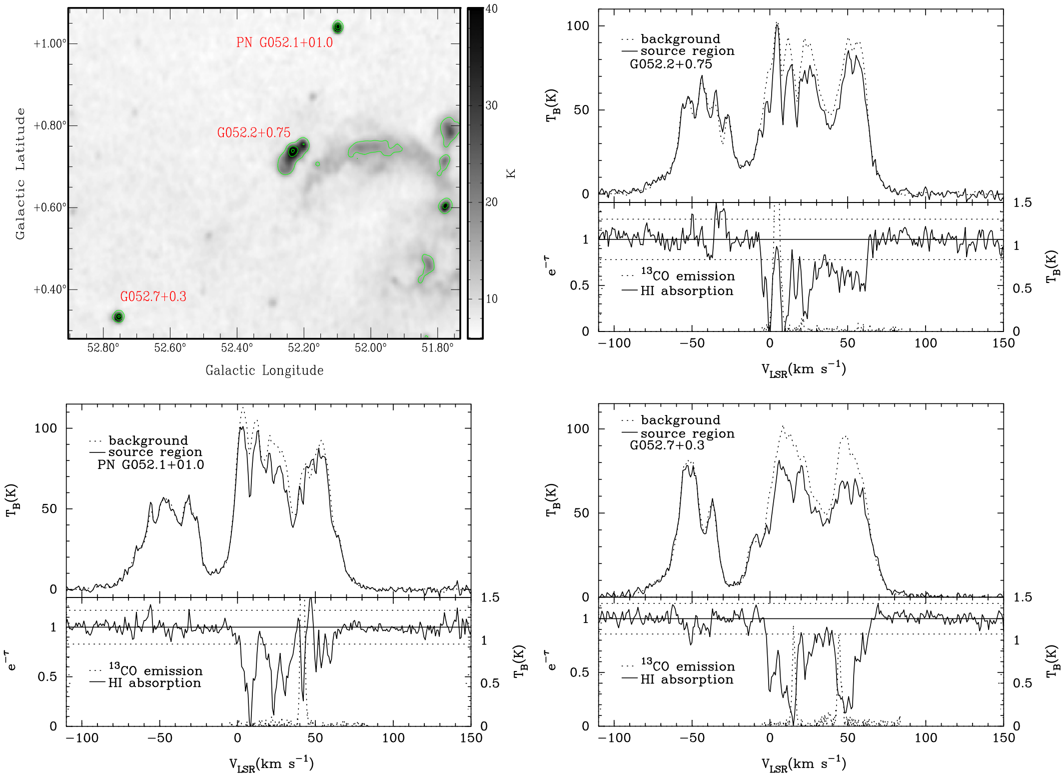

Figure 6. 1420 MHz continuum image of PN G052.1+01.0, and its background sources (top left), and the H I spectra of PN G052.1+01.0 (bottom left), G052.2 +0.75 (top right), and G052.7+0.3 (bottom right). The map has superimposed contours (15, 35, 55 K) of the 1420 MHz continuum emission.

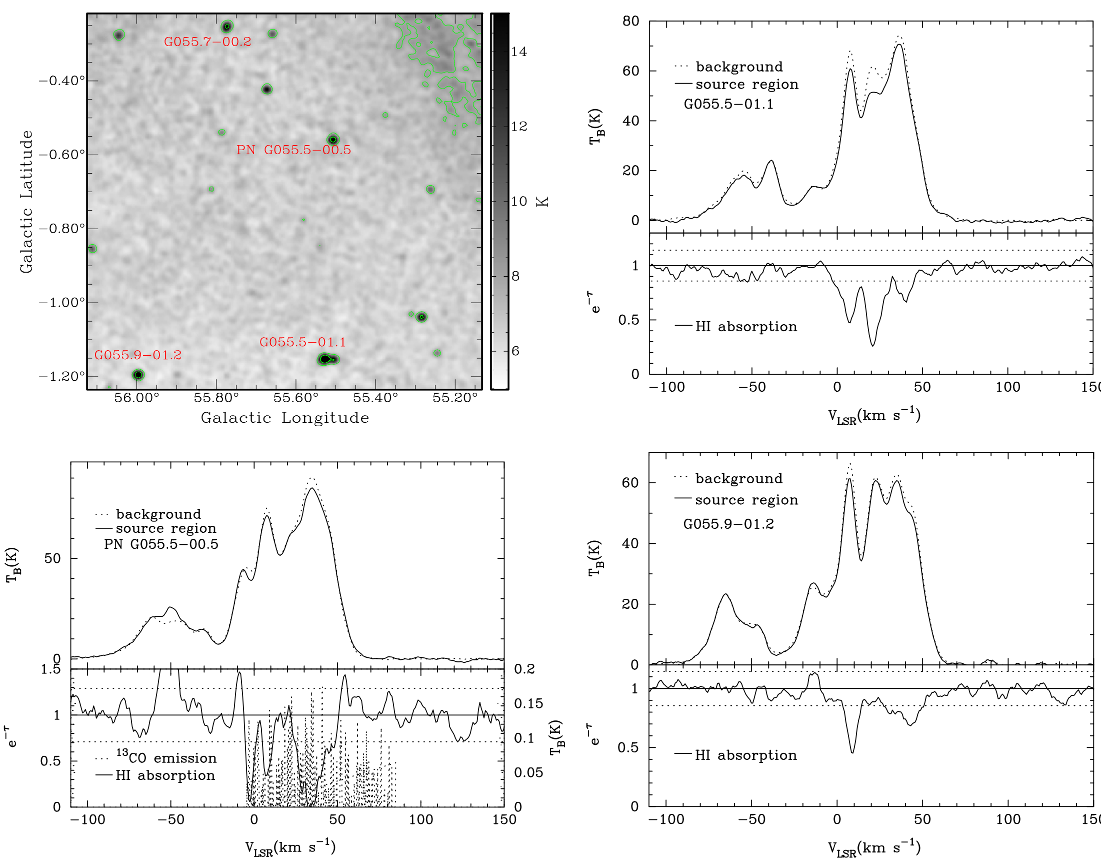

Figure 7. 1420 MHz continuum image of PN G055.5−00.5 and its nearby background sources (top left), and the H I spectra of PN G055.5−00.5 (bottom left), G055.5−01.1 (top right), and G055.9−01.2 (middle right). The H I spectra of G055.7−00.2 is shown in Figure 21. The map has superimposed contours (8, 15, 35 K) of the 1420 MHz continuum emission.

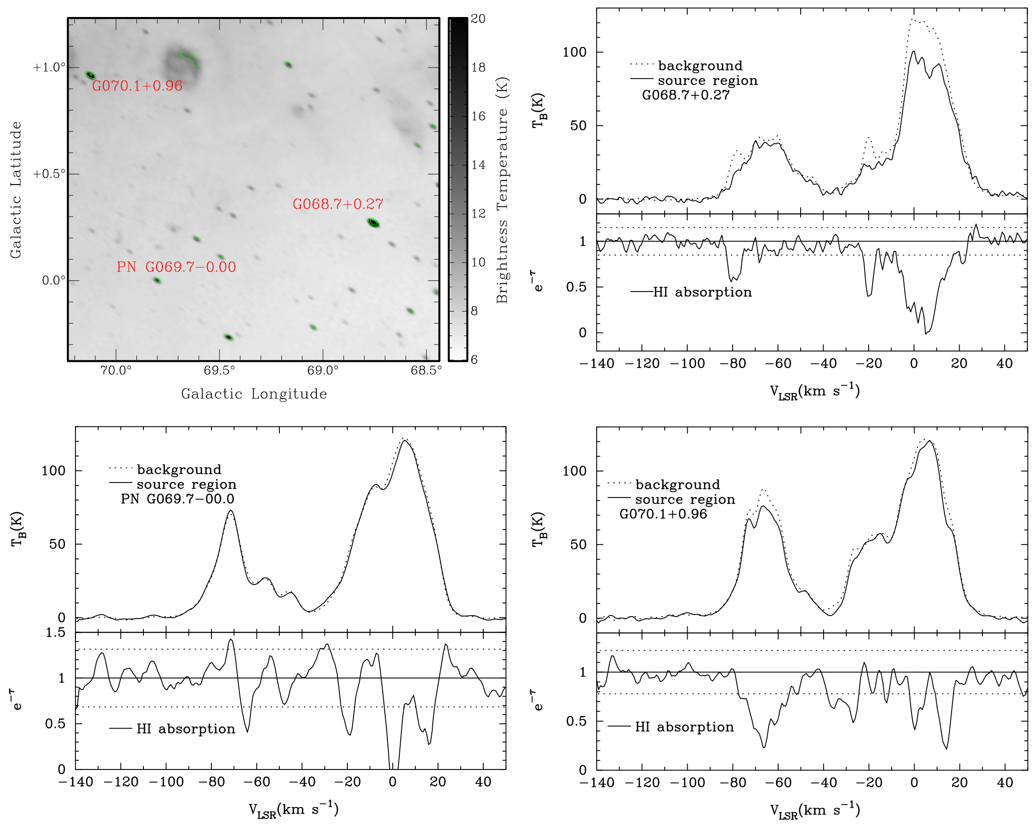

Figure 8. 1420 MHz continuum image of PN G069.7−00.0, and its nearby background sources (top left), and the H I spectra of PN G069.7−00.0 (bottom left), G068.7+0.27 (top right), and G070.1+0.96 (bottom right). The map has superimposed contours (5, 12, 32 K) of the 1420 MHz continuum emission.

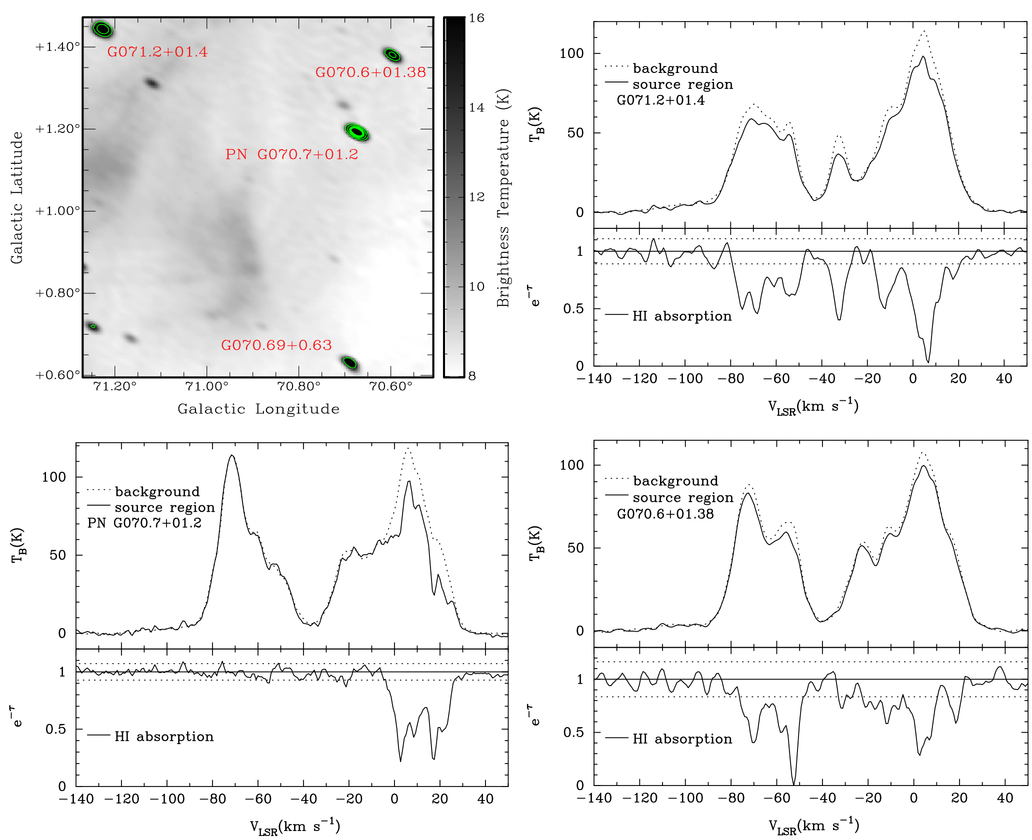

Figure 9. 1420 MHz continuum image of PN G070.7+01.2, and its background sources (top left), and the H I spectra of PN G070.7+01.2 (bottom left), G071.2 +01.4 (top right), and G070.6+01.38 (bottom right). The H I spectra of G070.69+0.63 is listed in Figure 21. The map has superimposed contours (15, 25, 50 K) of the 1420 MHz continuum emission.

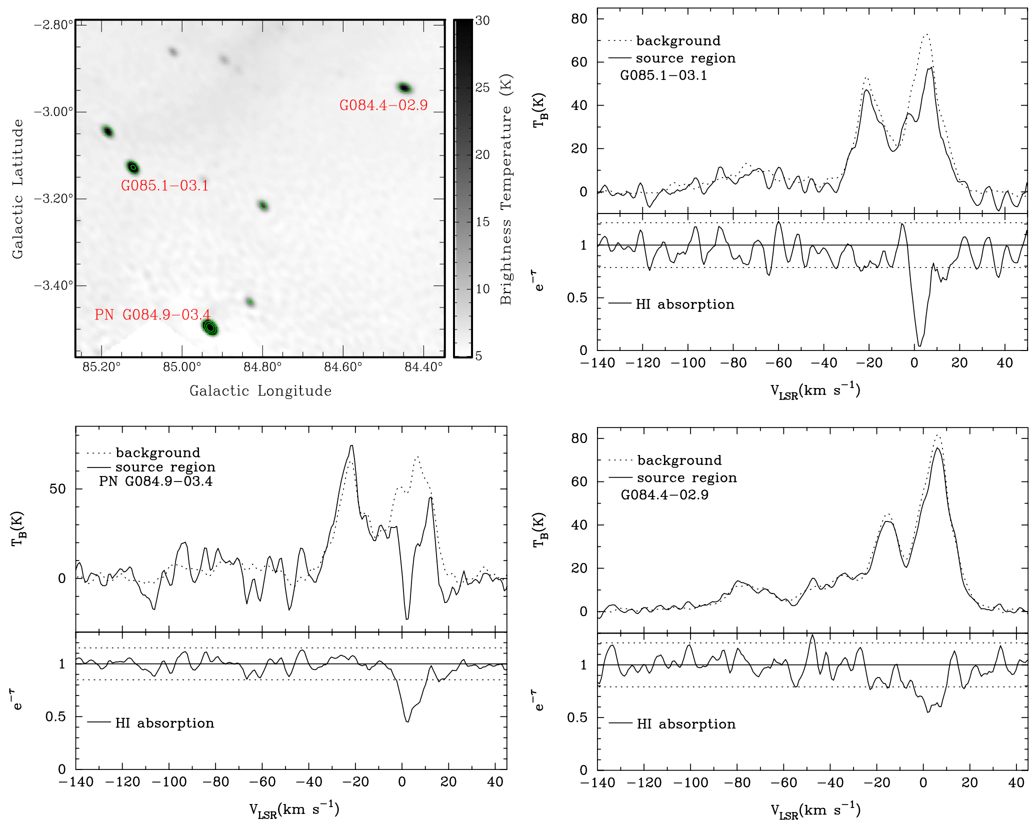

Figure 10. 1420 MHz continuum image of PN G084.9−03.4 and its nearby background sources (top left), and the H I spectra of PN G084.9−03.4 (bottom left), G085.1−03.1 (top right), and G084.4−02.9 (bottom right). The map has superimposed contours (15, 50, 100 K) of the 1420 MHz continuum emission.

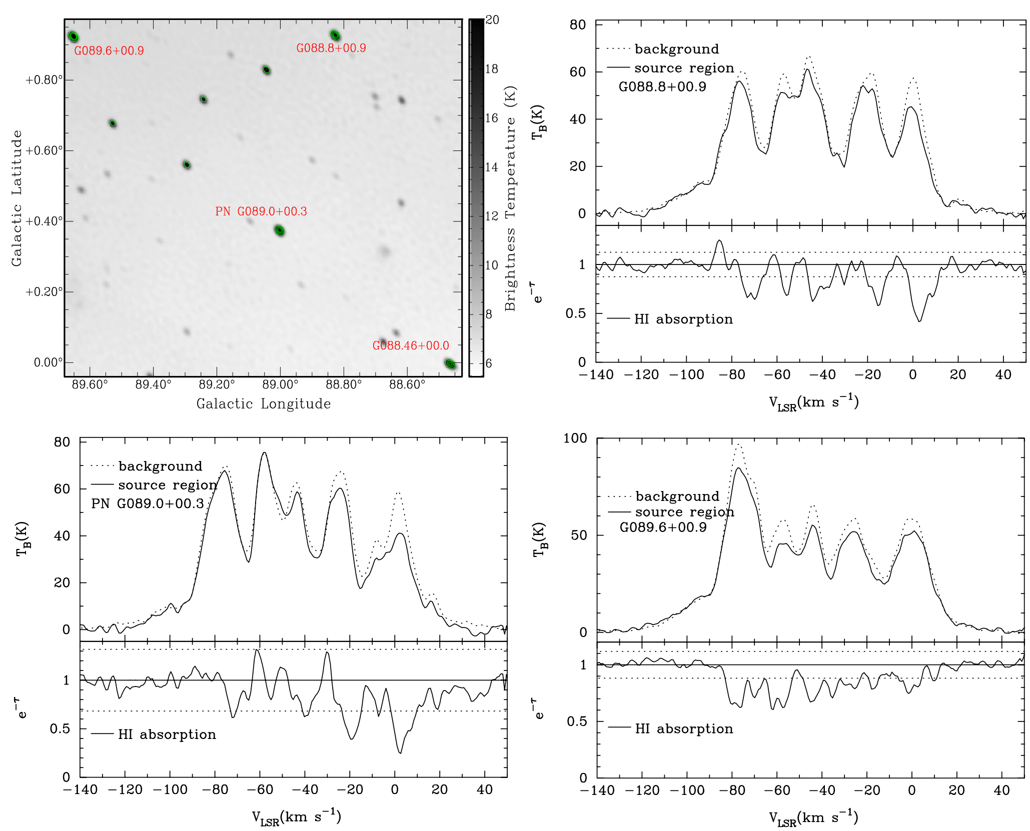

Figure 11. 1420 MHz continuum image of PN G089.0+00.3 and its nearby background sources (top left), and the H I spectra of PN G089.0+00.3 (bottom left), G088.8+00.9 (top right), and G089.6+00.9 (bottom right). The H I spectra of G088.46+00.0 is shown in Figure 21. The map has superimposed contours (15, 25, 35 K) of the 1420 MHz continuum emission.

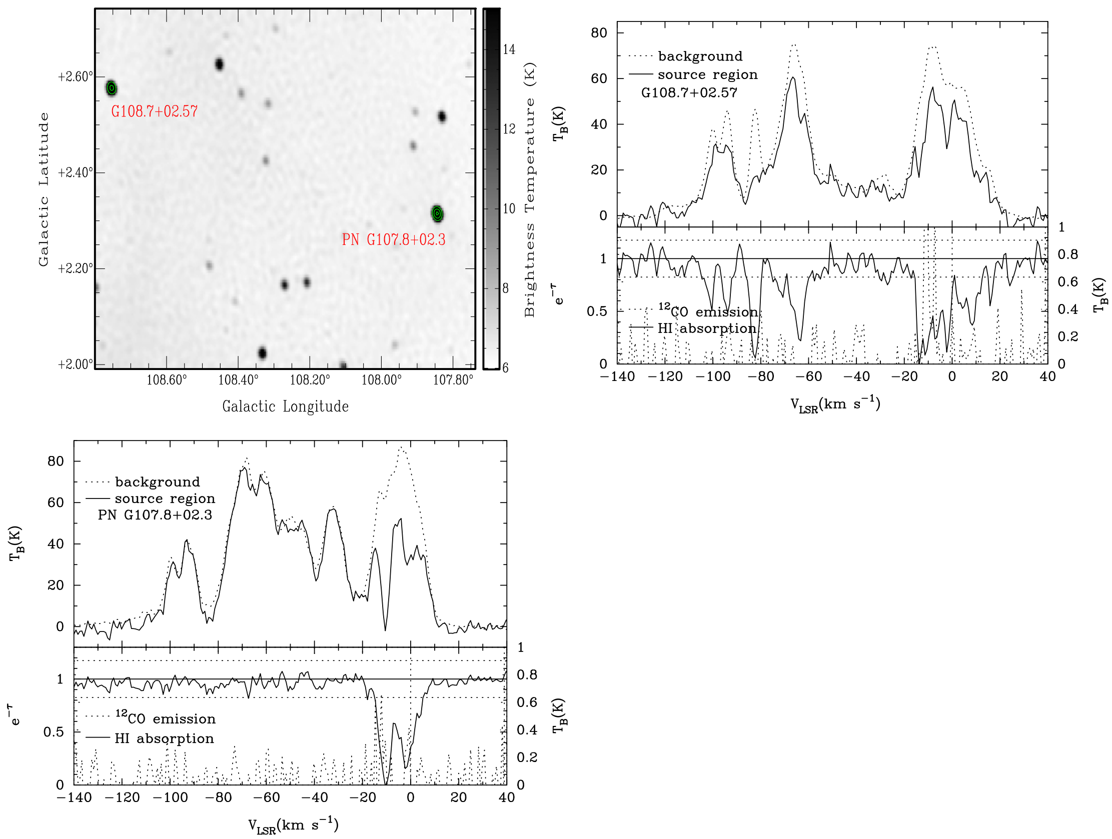

Figure 12. 1420 MHz continuum image of PN G107.8+02.3 and its nearby background sources (top right), and the H I spectra of PN G107.8+02.3 (bottom left) and G108.7+02.57 (top right). The map has superimposed contours (20, 50, 100 K) of the 1420 MHz continuum emission.

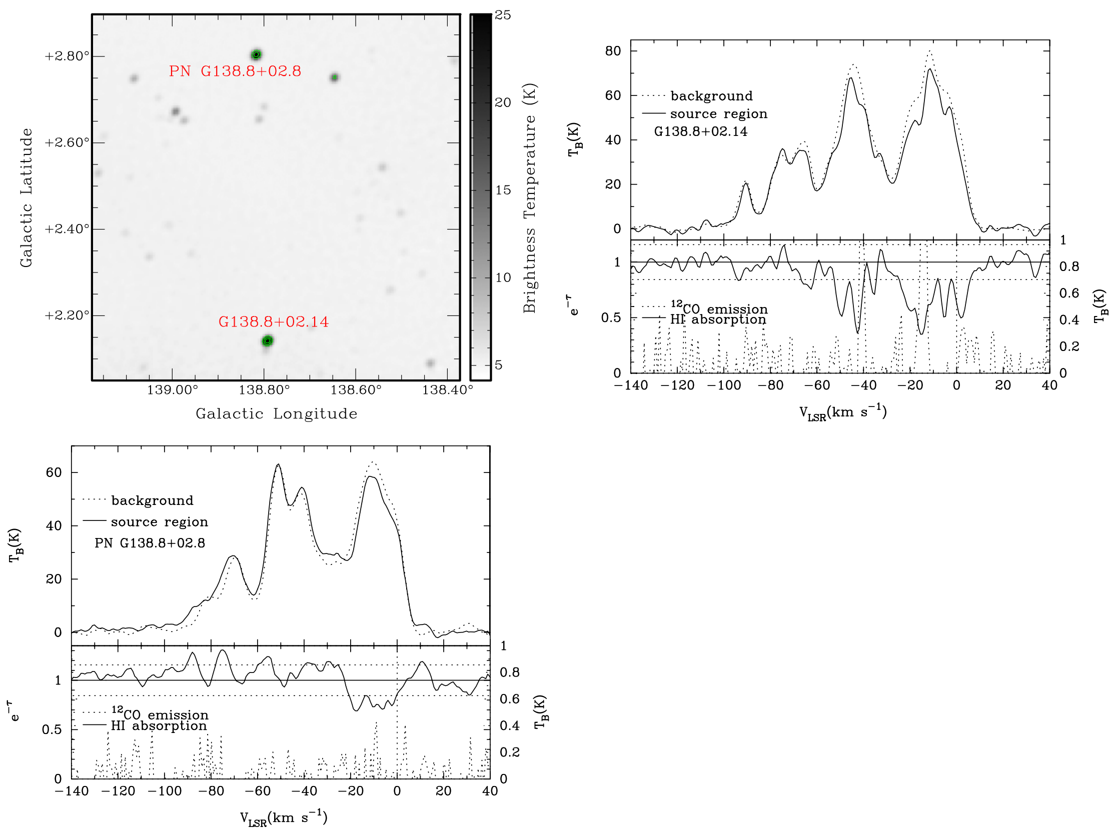

Figure 13. 1420 MHz continuum image of PN G138.8+02.8 and G138.8+02.4 (top left), and the H I spectra of PN G138.8+02.8 (bottom left) and G138.8+02.14 (top right). The map has superimposed contours (15, 25, 35 K) of the 1420 MHz continuum emission.

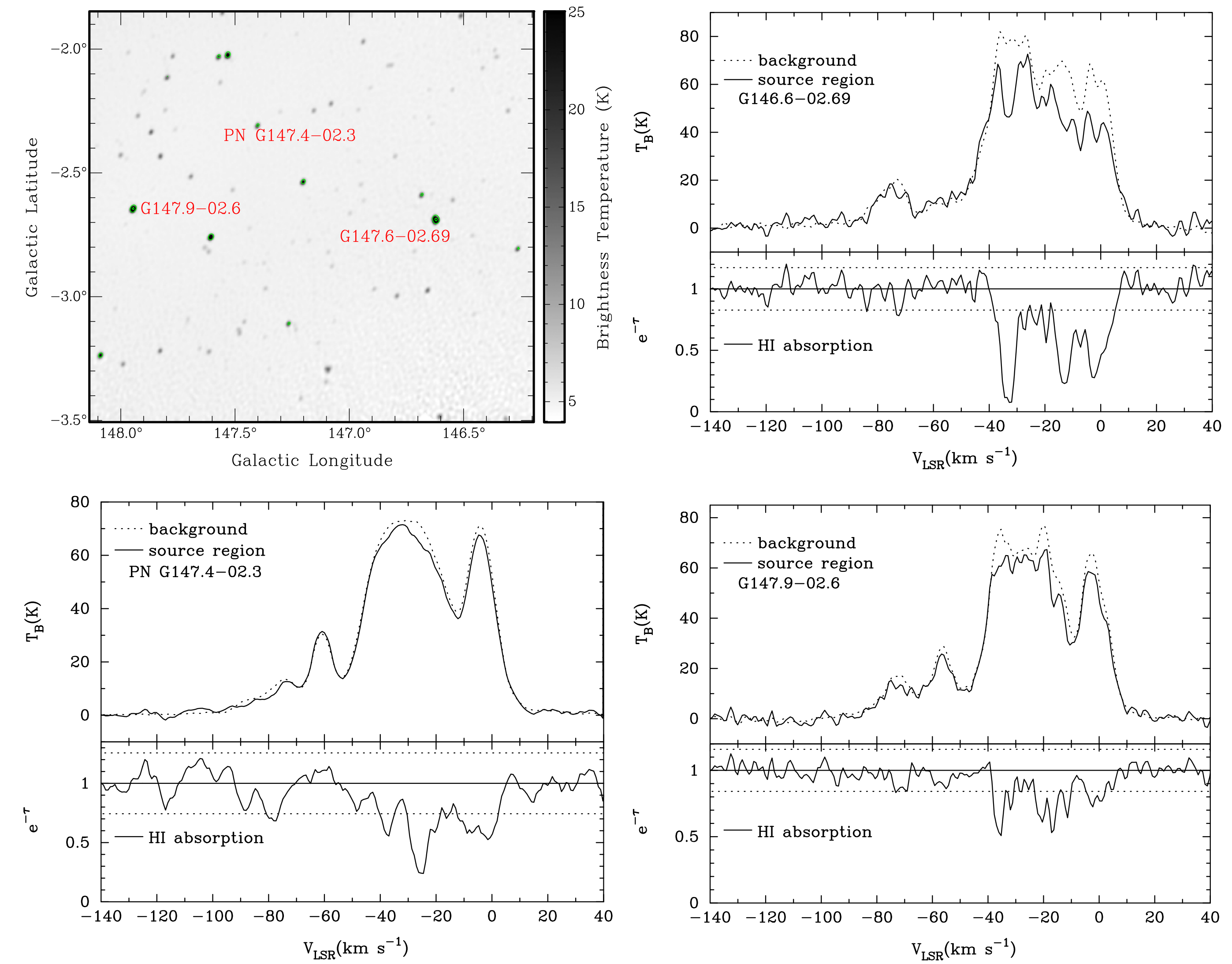

Figure 14. 1420 MHz continuum image of PN G147.4−02.3, and its background sources (top left), and the H I spectra of PN G147.4−02.3 (bottom left), G146.6 −2.69 (top right), and G147.9−02.6 (bottom right). The map has superimposed contours (15, 55 K) of the 1420 MHz continuum emission.

well as two nearby background sources, whereas its respective absorption feature is detected only in two background sources. This gives an upper limit distance of 4.3 ± 0.6 kpc for the PN. Hence, the distance of the PN is between ∼0.7 and 4.3 ± 0.6 kpc.

This PN, called NGC 7027 as the most luminous Galactic PN, has a distance measured by various methods, such as statistical distances (0.7 kpc, Maciel 1984; 0.63 kpc, van de Steene & Zijlstra 1995; 0.64 kpc, Zhang 1995), reddening (<1.15 kpc, Navarro et al. 2012), and expansion parallax (0.703 ± 0.095 kpc, Hajian et al. 1993; 0.98 ± 1.0 kpc, Zijlstra et al. 2008; 0.88 ± 0.15 kpc, Masson 1989; 0.68 ± 0.17 kpc, Mellema 2004). In fact, Pottasch et al. (1982) gave a upper limit distance of 4.5 kpc, which was also measured by comparing the H I absorption feature at $-20\ \mathrm{km\ s^{-1}}$ between the PN and a background source. So the lower limit distance 0.7 kpc is reliable for PN G084.9−03.4.

PN G089.0+00.3 (Figure 11).

The disagreement between the observed tangent point velocity ($10\ \mathrm{km\ s^{-1}}$) shown in Figure 11 and the expected value ($0.03\ \mathrm{km\ s^{-1}}$) may be due to random motions of H I clouds at the tangent point in the direction $l = 89°$. Figure 11 shows H I spectra of the PN and background sources. The absorption features at $-70\ \mathrm{km\ s^{-1}}$ and $-40\ \mathrm{km\ s^{-1}}$ are likely not real, and two significant absorption features at $-20\ \mathrm{km\ s^{-1}}$ and $\sim 0\ \mathrm{km\ s^{-1}}$ indicate that a reliable lower limit distance for this PN is 3.5 ± 0.6 kpc. No reliable upper limit distance can be determined for this PN.

The distance of this PN (also named NGC 7026) has been investigated previously by using H I absorption (2.5 ± 1.0 kpc, Gathier et al. 1986a), the statistical method (e.g., 2.35 kpc, Stanghellini et al. 2008; 2.03 kpc, Zhang 1995), reddening (e.g., 1.57 ± 0.65 kpc, Kaler & Lutz 1985; 2.3 kpc, Pottasch 1983), the surface gravity method (e.g., 3.5 kpc, Zhang 1993; 4.2 kpc, Cazetta & Maciel 2000), and the spectroscopic method (1.9 kpc, Gruendl et al. 2004). Our result is reasonably consistent with surface gravity distance and larger than others. Actually, Gathier et al. (1986a) found a weak absorption at $\sim -20\ \mathrm{km\ s^{-1}}$ in the PN spectrum, but they did not take this absorption as clear evidence to constrain its distance. The $-7\ \mathrm{km\ s^{-1}}$ absorption feature they chose for the lower limit distance of 2.5 ± 1.0 kpc is also detected in our data. Since our data has higher resolution and is more sensitive, the absorption

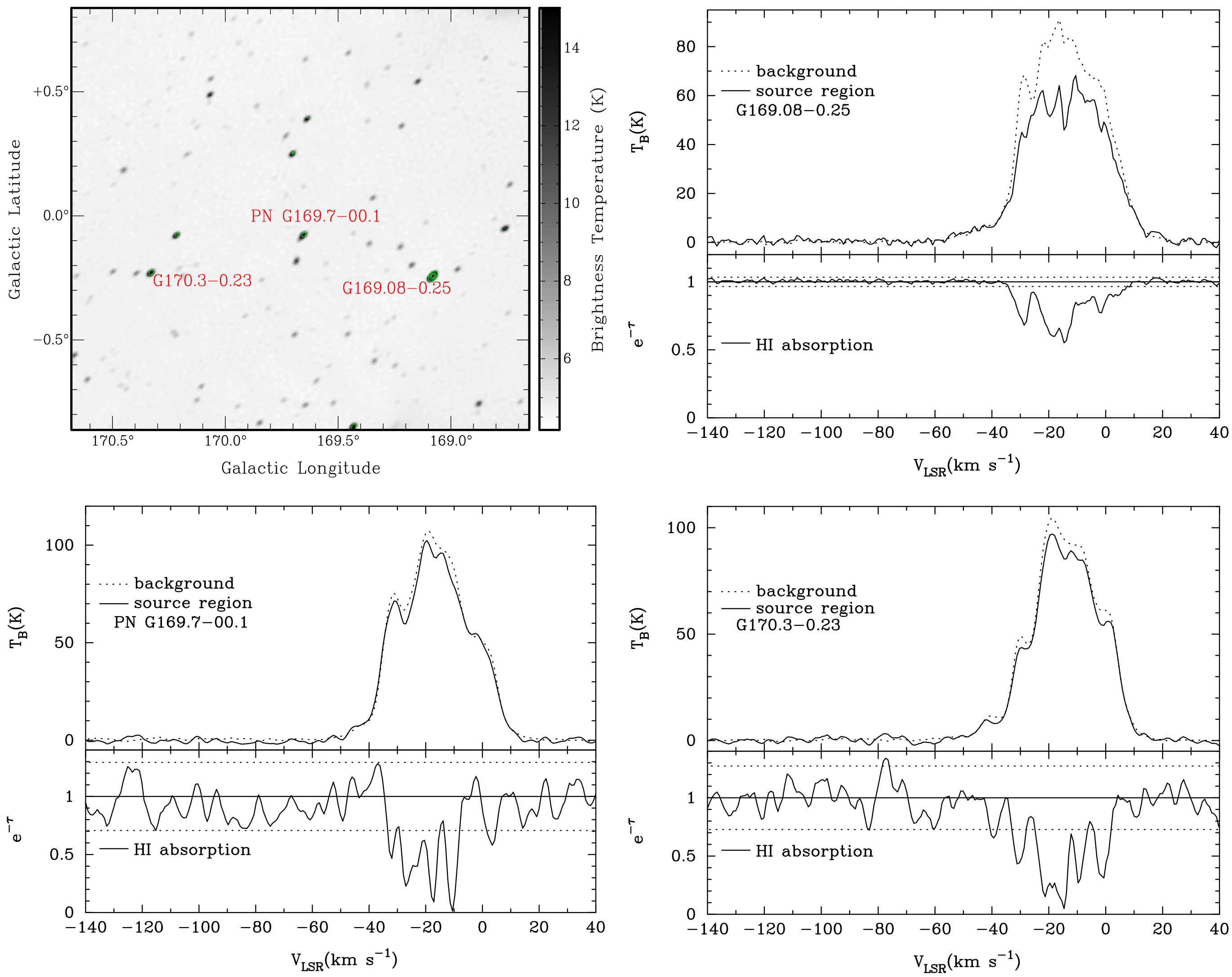

Figure 15. 1420 MHz continuum image of PN G169.7−00.1 and its background sources (top left), and the H I spectra of PN G169−00.1 (bottom left), G169.08 −0.25 (top right), and G170.3−0.23 (bottom right). The map has superimposed contours (15, 50, 100 K) of the 1420 MHz continuum emission.

at $-20\ \mathrm{km\ s^{-1}}$ detected in our work can be used to determine a more reliable lower limit distance of 3.5 ± 0.6 kpc for this PN.

PN G107.8+02.3 (Figure 12).

The absorption features at positive velocities in both the PN and G108.7+02.57 are partly due to a cloud with anomalous motion. Clear absorption features are present at ~-30, ~-60, and $\sim-105\ \mathrm{km\ s^{-1}}$ in the spectrum of the background source G108.7+02.57, while no absorption features are detected at the velocities in the PN spectrum. This implies the PN is in front of the H I cloud at $\sim-30\ \mathrm{km\ s^{-1}}$, i.e., 2.8 ± 0.5 kpc. The CO emission, H I emission, and absorption features at $-12\ \mathrm{km\ s^{-1}}$ in the PN spectrum indicate a lower limit distance of 1.2 ± 0.6 kpc. Therefore, the distance of PN G107.8+02.3 is between 1.2 ± 0.6 and 2.8 ± 0.5 kpc.

For this PN, also called NGC 7354, the distance has been measured by various methods. Gathier et al. (1986a) suggested a H I absorption distance 1.5 ± 0.5, determined by the nearby H II regions of the PN. Giammanco et al. (2011) obtained a distance of 1.0 ± 0.15 kpc based on the distance-extinction relationship in the direction toward the PN. Zhang (1993) gave a distance of 2.1 kpc by the surface gravity method. The revised Shklovshy method suggested distances of 1.27 kpc by Cahn et al. (1992), 1.3 kpc by Zhang (1995), 1.23 kpc by van de Steene & Zijlstra (1995), 1.19 kpc by Phillips (2004), and 1.70 kpc by Stanghellini et al. (2008). So the lower distance of 1.2 ± 0.6 kpc seems reasonable for the PN.

PN G138.8+02.8 (Figure 13).

There are clear H I absorption and CO emission features at $-42\ \mathrm{km\ s^{-1}}$ in the direction of G138.8+02.14, while similar absorption is not detected in the PN spectrum. This indicates that the PN is in front of the H I cloud at $-42\ \mathrm{km\ s^{-1}}$. The PN spectrum reveals one reliable H I absorption feature at $-20\ \mathrm{km\ s^{-1}}$. Therefore, we obtain a lower limit distance of 1.6 ± 0.5 kpc and an upper limit distance of 3.8 ± 0.8 kpc.

PN G138.8+02.8 (also called IC 289) has statistical distances of 1.43 kpc by Cahn et al. (1992), 1.68 kpc by Zhang (1995), 1.45 kpc by Stanghellini et al. (2008), 1.18 kpc by Phillips (2004), and 1.48 kpc by van de Steene & Zijlstra (1995), as well as a reddening distance of 2.71 ± 0.195 kpc (Kaler & Lutz 1985). So we suggest a distance of 1.6 ± 0.5 kpc for the PN.

PN G147.4−02.3 (Figure 14).

Both H I emission and absorption features at $-35\ \mathrm{km\ s^{-1}}$ appear in the spectra of the PN as well as its nearby background

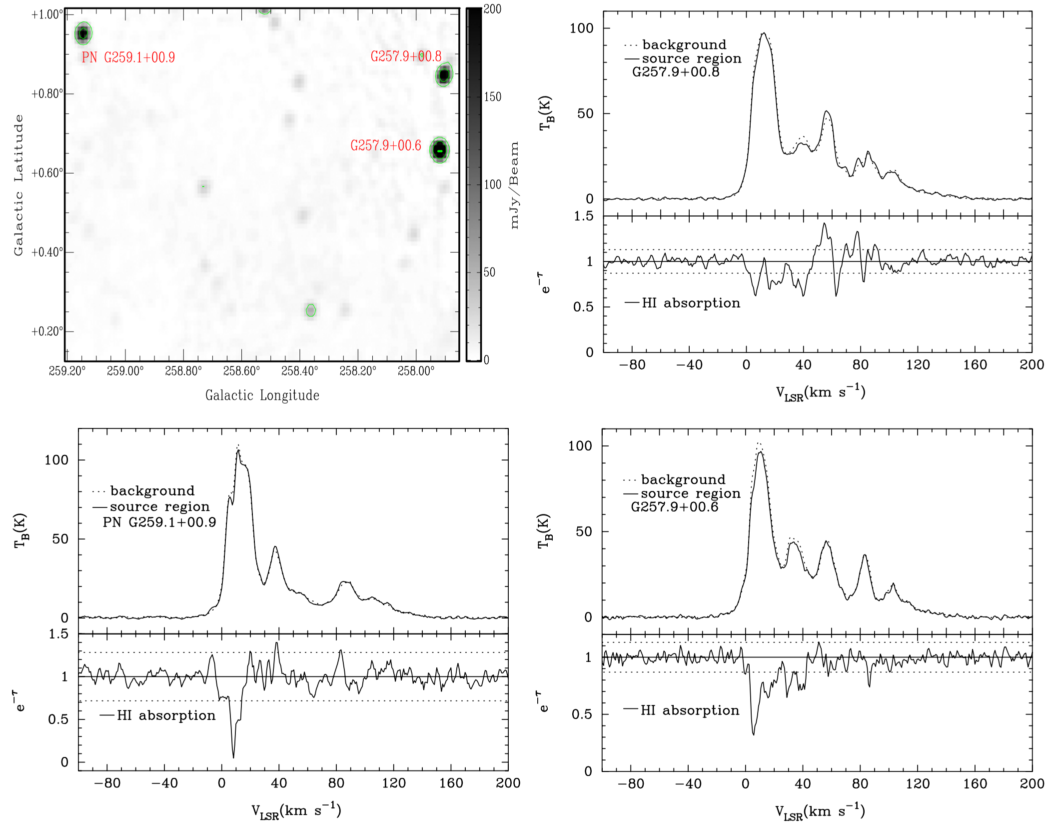

Figure 16. 1420 MHz continuum image of PN G259.1+00.9, and its nearby background sources (top left), and the H I spectra of PN G259.1+00.9 (bottom left), G257.9+00.8 (top right), and G257.9+00.6 (bottom right). The map has superimposed contours (0.03, 0.15, 0.5 Jy) of the 1420 MHz continuum emission.

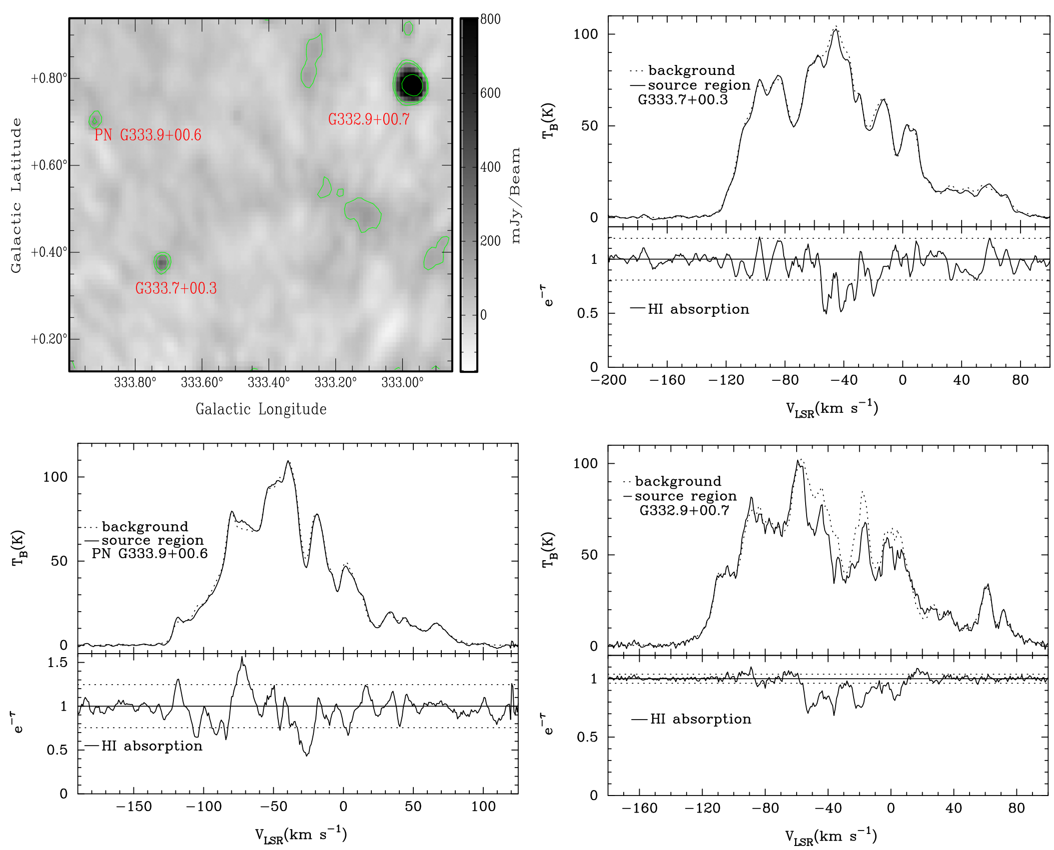

Figure 17. 1420 MHz continuum image of PN G333.9+00.6, and its background sources (top left), and the H I spectra of PN G333.9+00.6 (bottom left), G333.7 +00.3 (top right), and G332.9+00.7 (bottom right). The map has superimposed contours (0.1, 0.18, 1.0 Jy) of the 1420 MHz continuum emission.

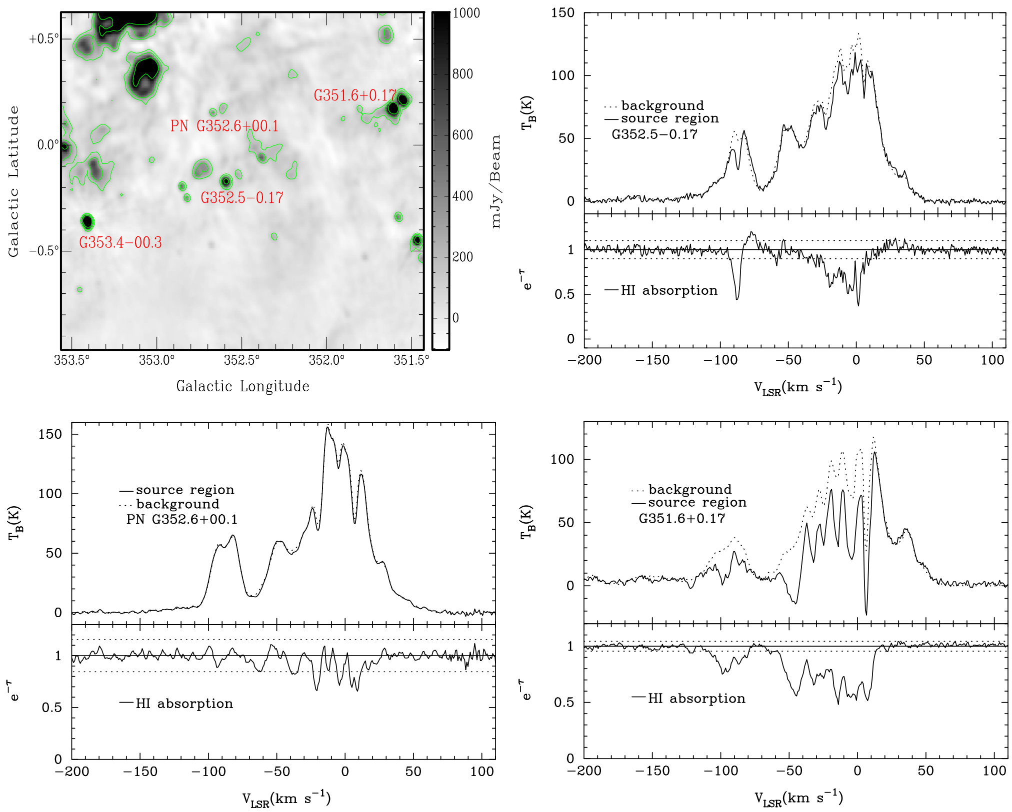

Figure 18. 1420 MHz continuum image of PN G352.6+00.1 and its nearby background sources (top left), and the H I spectra of PN G352.6+00.1 (bottom left), G352.5−0.17 (top right), and G351.6+0.17 (bottom right). The H I spectra of G353.4−00.3 is shown in Figure 19. The map has superimposed contours (0.15, 0.35, 1.0 Jy) of the 1420 MHz continuum emission.

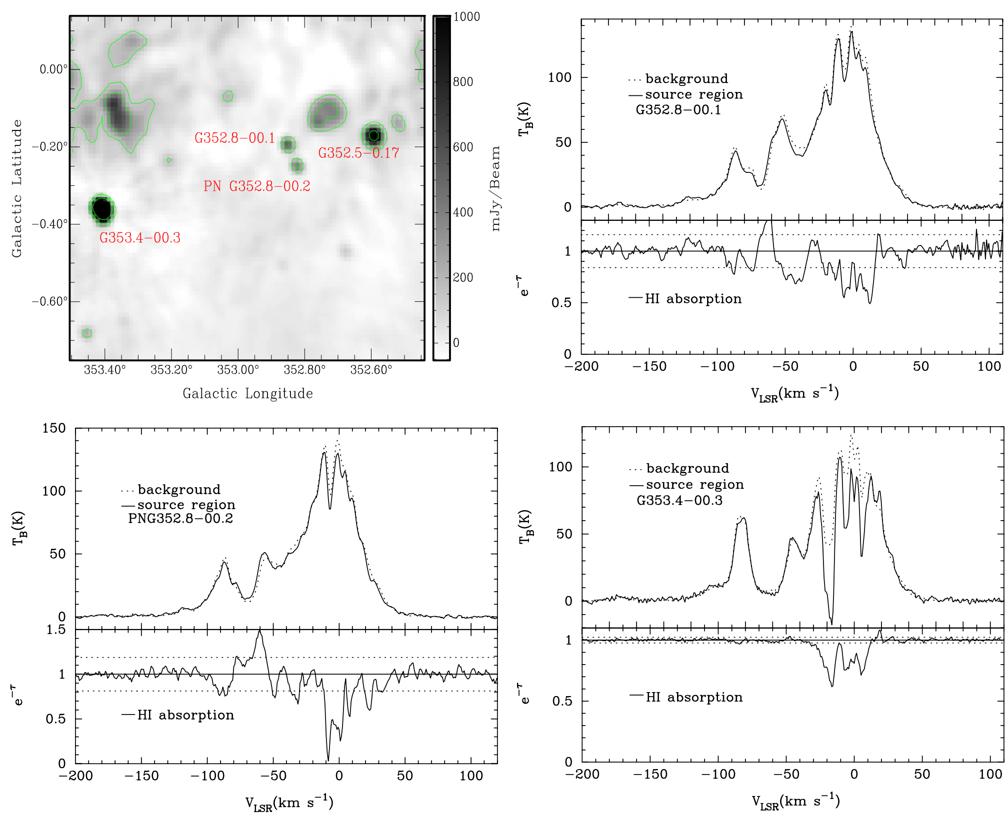

Figure 19. 1420 MHz continuum image of PN G352.8−00.2 and its nearby background sources (top left), and the H I spectra of PN G352.8−00.2 (bottom left), G352.8−00.1 (top right), and G353.4−00.3 (bottom right). The H I spectra of G352.5−0.17 is shown in Figure 18. The map has superimposed contours (0.15, 0.35, 1.0 Jy) of the 1420 MHz continuum emission.

Table 2
Final Kinematic Distances of Planetary Nebulae

PN G Name	PN Name	Distance Limits (kpc)	Final Distance (kpc)	Distance by Others(Ref.) (kpc)	Method
				2.4 (C01)	surface gravity
				1.75 (C92), 1.66 (S95)	statistical
G020.9−01.1	M 1−51	3.1 ± 0.3−7.1 ± 0.6	3.1 ± 0.3	1.74 (Z95), 2.29 (S08)	statistical
				1.59 (Ph04)	statistical
				2.31 ± 0.75 (F16)	statistical
G029.0+00.4	A66 48	3.5 ± 0.3−6.6 ± 1.0	3.5 ± 0.3	1.2 (M84)	statistical
				1.41 ± 0.43 (F16)	statistical
G030.2−00.1	…	10.9 ± 0.3−13.2 ± 0.5	10.9 ± 0.3−13.2 ± 0.5	…	…
G051.5+00.2	KLW 1	4.7 ± 1.4−9.5 ± 0.4	4.7 ± 1.4−9.5 ± 0.4	…	…
G052.1+01.0	…	4.7 ± 1.4−5.4 ± 0.7	4.7 ± 1.4−5.6 ± 0.8	…	…
				1.66 (C92), 3.68 (S08)	statistical
G055.5 − 00.5	M 1−71	4.3 ± 1.5−8.6 ± 0.4	4.3 ± 1.5	3.17 (Z95), 3.17 (S95)	statistical
				2.88 ± 0.91 (F16)	statistical
				2.9 ± 0.4 (G11)	reddening
				3.31 (C92), 4.23 (S08)	statistical
G069.7 − 00.0	K 3−55	11.07 ± 0.61−12.02 ± 0.67	?	3.26 (Z95), 3.09 (S95)	statistical
				2.96 (Ph04)	statistical
				3.54 ± 1.32 (F16)	statistical
G070.7+01.2	M 3−60	2.5 ± 1.6−5.0 ± 0.7	5.0 ± 0.7	4.5 ± 1.0 (B89)	H i absorption
				0.7 (M84), 0.64 (Z95)	statistical
				0.27 (C92), 0.63 (S95)	statistical
				0.94 ± 0.27 (F16)	statistical
				2.3−2.9 (C01)	surface gravity
G084.9−03.4	NGC 7027	0.7−4.3 ± 0.6	0.7	0.703 ± 0.095 (H93)	expansion parallax
				0.98 ± 1.0 (Z08)	expansion parallax
				0.94 ± 0.2 (M86)	expansion parallax
				0.88 ± 0.15 (M89)	expansion parallax
				0.68 ± 0.17 (M04)	expansion parallax
				<1.15 (N12)	reddening
				<4.5 (P82)	H i absorption
				2.5 ± 1.0 (G86)	H i absorption
				1.9 (C92), 2.35 (S08)	statistical
				2.03 (Z95), 1.91 (Ph04)	statistical
				1.94 (S95)	statistical
G089.0+00.3	NGC 7026	⩾3.5 ± 0.6	3.5 ± 0.6	1.67 ± 0.48 (F16)	statistical
				1.57 ± 0.65 (K85)	reddening
				2.3 (P83), <1.5 (G11)	reddening
				3.5 (Z93), 4.2 (C00)	surface gravity
				1.9 (G04)	Spectroscopic parallax
				1.5 ± 0.5(G86)	H i absorption
				1.27 (C92), 1.19 (Ph04)	statistical
				1.3 (Z95), 1.70 (S08)	statistical
				1.23 (S95)	statistical
G107.8+02.3	NGC 7354	1.2 ± 0.6−2.8 ± 0.5	1.2 ± 0.6	1.26 ± 0.37 (F16)	statistical
				1.0 ± 0.15 (G11)	reddening
				3.43 ± 0.62 (K85)	reddening
				2.1 (Z93), 3.2 (C00)	surface gravity
				2.71 ± 0.195 (K85)	reddening
				1.43 (C92), 1.45 (S08)	statistical
G138.8+02.8	IC 289	1.6 ± 0.6−3.8 ± 0.6	1.6 ± 0.6	1.68 (Z95), 1.18 (Ph04)	statistical
				1.48 (S95)	statistical
				1.88 ± 0.58 (F16)	statistical
				2.2−3.1 (C01)	surface gravity
				2.99 (C92), 3.36 (S95)	statistical
				3.53 (Z95), 3.39 (Ph04)	statistical
G147.4−02.3	M 1−4	3.6 ± 0.9−8.7 ± 1.7	3.6 ± 0.9	6.6 (S08)	statistical
				5.18 ± 1.55 (F16)	statistical
				3.3 ± 0.35 (G11)	reddening
				1.37 (C92), 1.388 (S08)	statistical
G169.7−00.1	IC 2120	⩾14.7	?	1.86 (Z95), 1.26 (Ph04)	statistical
				0.9 (C92), 1.07 (Z95)	statistical
G259.1+00.9	Hen 2−11	1.6 ± 0.6−2.4 ± 0.6	1.6 ± 0.6	0.80 ± 0.24 (F16)	statistical
				0.7 (J14)	Spectroscopic

Table 2
(Continued)

PN G Name	PN Name	Distance Limits (kpc)	Final Distance (kpc)	Distance by Others(Ref.) (kpc)	Method
G333.9+00.6	PMR 5	⩾1.9 ± 0.4	1.9 ± 0.4	1.0−1.5 (M03)	Spectroscopic
				>0.9 (M84)	statistical
G352.6+00.1	H 1−12	3.2 ± 0.8−5.0 ± 0.3	3.2 ± 0.8	1.40 (Z95), 1.37 (S95)	statistical
				2.42 ± 0.84 (F16)	statistical
				0.8 (M84), 1.36 (Ph04)	statistical
G352.8 − 00.2	H 1−13	2.1 ± 0.9−3.2 ± 0.8	2.1 ± 0.9	1.53 (C92), 1.39 (Z95)	statistical
				1.34 (S95)	statistical
				1.74 ± 0.59 (F16)	statistical

Reference. C01, Cazetta & Maciel (2001); C92, Cahn et al. (1992); S95, van de Steene & Zijlstra (1995); Z95, Zhang (1995); S08, Stanghellini et al. (2008); B89, Bally et al. (1989); N12, Navarro et al. (2012); G11, Giammanco et al. (2011); K85, Kaler & Lutz (1985); G86, Gathier et al. (1986a); C00, Cazetta & Maciel (2000); G04, Gruendl et al. (2004); P83, Pottasch (1983); Z08, Zijlstra et al. (2008); H93, Hajian et al. (1993); M84, Maciel (1984); Z93, Zhang (1993); Ph04, Phillips (2004); M04, Mellema (2004); M86, Masson (1986); M03, Morgan et al. (2003); M89, Masson (1989); J14, Jones et al. (2014); P82, Pottasch et al. (1982); F16, Frew et al. (2016); *?*—represents that the distances are an open question.

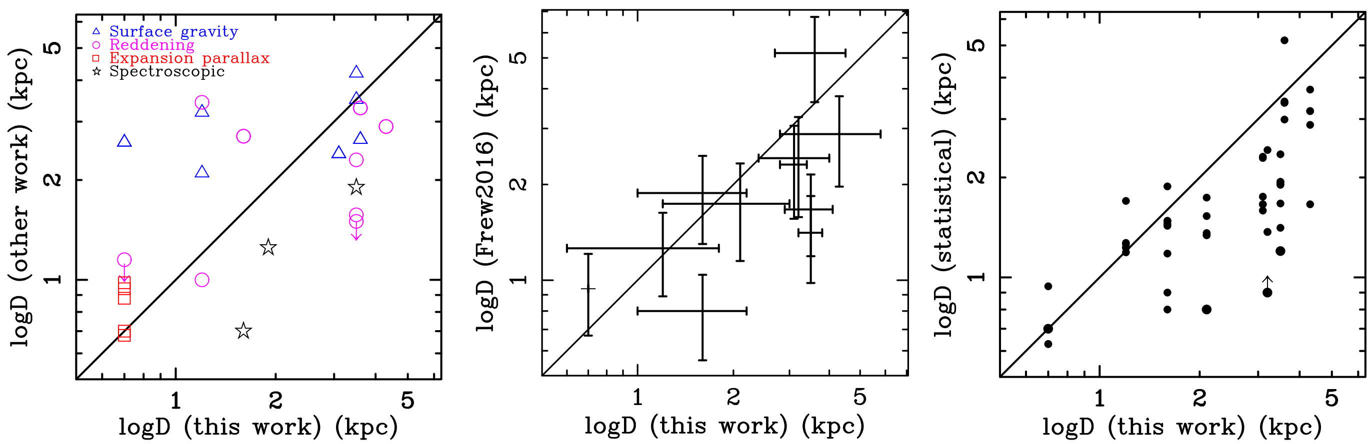

Figure 20. Left panel: the correlation between our work and all other work (except the statistical method). Middle panel: the correlation between our work and Frew et al. (2016). Right panel: the correlation between our work and all statistical results.

sources. This implies that the PN is behind the H I cloud at 3.6 ± 0.9 kpc. In addition, the presence of clear H I emission and the absence of absorption at −60 km s^{-1} in the PN spectrum indicates that the PN is in front of the H I cloud at 8.7 ± 1.7 kpc. Overall, the distance of the PN is between 3.6 ± 0.9 kpc and 8.7 ± 1.7 kpc.

The distance of the PN was measured by several methods previously, i.e., a surface gravity distance of 2.2−3.1 kpc by Cazetta & Maciel (2001), the revised Shklovsky distances of 3.39 kpc by Phillips (2004) and 3.53 kpc by Zhang (1995), as well as a reddening distance of 3.3 ± 0.35 kpc by Giammanco et al. (2011). These are consistent with our lower limit distance 3.6 ± 0.9 kpc.

PN G169.7−00.1 (Figure 15).

This PN is most likely a H II region, as suggested by Zijlstra et al. (1990), which is close to the Galactic plane (see Figure 15). The H I emission and absorption features at −32 km s^{-1} in the spectra of the PN and the background sources imply they are beyond the H I cloud at ~14.7 kpc; see Figure 1 (upper right panel). This lower limit distance is derived by considering the average random velocity 6 km s^{-1} of H I clouds. No upper limit distance can be derived. Our lower limit is much larger than previous measurements, i.e., 1.37 kpc by Cahn et al. (1992), 1.86 kpc by Zhang (1995), 1.26 kpc by Phillips (2004), and 1.39 kpc by Stanghellini et al. (2008). So we prefer to keep its distance an open question.

PN G259.1+00.9 (Figure 16).

There is strong continuous H I emission and absorption between 0 to 12 km s^{-1} in the PN spectrum (Figure 16), but no absorption features appear up to the tangent point velocity after 12 km s^{-1} ($3\sigma = 0.27$). This means that the PN is beyond the nearside for 12 km s^{-1}, i.e., 1.6 ± 0.6 kpc. Unlike the PN spectrum, the two background sources show absorption features at velocities of 20 and 40 km s^{-1}. This implies that the PN is in front of the H I at 20 km s^{-1}, i.e., 2.4 ± 0.6 kpc. So the distance of the PN is between 1.6 ± 0.6 kpc and 2.4 ± 0.6 kpc. In comparison with previous work obtained by the statistical method (0.9 kpc, Cahn et al. 1992; 1.07 kpc, Zhang 1995) and spectroscopic distance (0.7 kpc Jones et al. 2014), we suggest a distance of 1.6 ± 0.6 kpc for this PN.

PN G333.9+00.6 (Figure 17).

Figure 17 shows that this PN has a poor absorption spectrum. One possible absorption feature at −26 km s^{-1} can be used to provide a lower limit distance of 1.9 ± 0.4 kpc. No upper limit distance can be derived for the PN. In fact, the previous spectroscopic distance (1.0−1.5 kpc) obtained by Morgan et al. (2003) agrees with our result. This PN likely has a distance of 1.9 ± 0.4 kpc.

PN G352.6+00.1 (Figure 18).

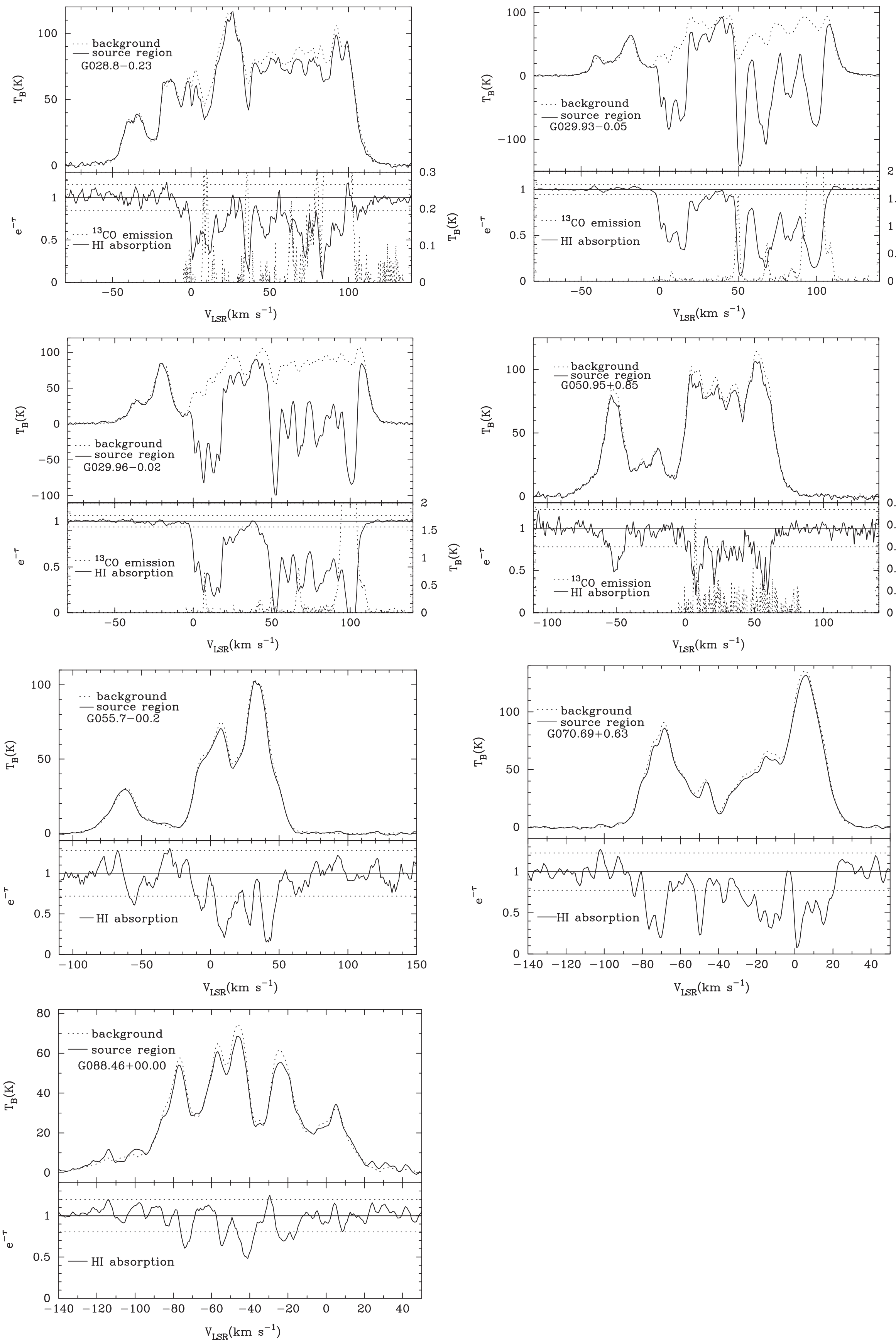

Figure 21. Nearby background sources are also used to measure the PN kinematic distances. The dotted horizontal lines in the lower panel of the background sources show the 3σ noise level.

Two background sources (G352.5−0.17, G351.6+0.17) show reliable absorption features at the tangent point velocity, while this does not appear in the PN spectrum. This implies that the PN is in front of the tangent point. H i emission and absorption appear at $-20\,\mathrm{km\,s^{-1}}$ in the spectra of the PN and H ii region G353.4−00.3. In fact, the PN is behind the H ii region G353.4−00.3 (3.2 ± 0.8 kpc, Tian et al. 2008). In addition, an absorption feature at $-50\,\mathrm{km\,s^{-1}}$ is seen in the spectrum of G351.6+0.17, while H i emission is seen but no absorption at the same velocity in the PN spectrum. This implies the PN is in front of the near distance of $-50\,\mathrm{km\,s^{-1}}$, i.e., 5.0 ± 0.3 kpc. So PN G352.6+00.1 is between 3.2 ± 0.8 kpc and 5.0 ± 0.3 kpc.

Maciel (1984) gave a lower limit 0.9 kpc for this PN by assuming a relationship between the nebular ionized mass and radius. Zhang (1995) and van de Steene & Zijlstra (1995) suggested distances of 1.40 and 1.37 kpc based on the revised relation between radio surface brightness temperature and nebula radius. Therefore, we adopt 3.2 ± 0.8 kpc for the PN.

PN G352.8−00.2 (Figure 19).

The weak absorption features at the tangent velocity, −36, and $-90\,\mathrm{km\,s^{-1}}$ in the H i spectrum of PN G352.8−00.2 have an S/N of about 3σ (0.24), so we do not regard it as real absorption. The absorption feature at $-20\,\mathrm{km\,s^{-1}}$ is detected in the spectra of three background sources, but does not appear in the PN spectrum, implying the PN is in front of H i (3.2 ± 0.8 kpc, Tian et al. 2008). In addition, the presence of clear H i emission and the absence of an absorption feature at $-10\,\mathrm{km\,s^{-1}}$ in the PN spectrum reveals an lower limit distance of 2.1 ± 0.9 kpc for the PN. We conclude that the distance of the PN is between 2.1 ± 0.9 kpc and 3.2 ± 0.8 kpc.

The distance of the PN was also suggested by statistical methods (e.g., 0.8 kpc, Maciel 1984; 1.36 kpc, Phillips 2004; 1.53 kpc, Cahn et al. 1992; 1.39 kpc, Zhang 1995; 1.34 kpc, van de Steene & Zijlstra 1995). Hence, we prefer the distance of 2.1 ± 0.9 kpc for the PN.

4. SUMMARY

We analyze the H i absorption spectra of 18 Galactic plane PNs and estimate their kinematic distances in this paper. The final results are shown in Table 2. We compare new kinematic distances of 15 PNs with the previous results determined from other methods, such as surface gravity (5 PNs, e.g., Zhang 1993; Cazetta & Maciel 2000), expansion parallax (1 PN, e.g., Hajian et al. 1993; Zijlstra et al. 2008), reddening (5 PNs, e.g., Kaler & Lutz 1985; Giammanco et al. 2011), statistical (13 PNs, e.g., Cahn et al. 1992; Zhang 1995), and H i absorption (4 PNs, e.g., Gathier et al. 1986a; Bally et al. 1989). By considering the additional distance information, we determine distances for 13 PNs with uncertainties ranging from 10% to 50%. For 8 out of 13 PNs, the kinematic distances are determined with uncertainties less than 25%. For 3 objects (PN G020.9−01.1, PN G029.0+00.4, PN G084.9−03.4) the kinematic distances are derived with uncertainties less than 10%, and for the other 10 cases the kinematic distances are estimated with uncertainties less than 50%. This is a significant improvement compared with most of the previous measurements with uncertainties of two or three factors smaller. For three cases, the kinematic distance are derived with lower and upper distance limits (see Table 2). We do not suggest distances for PN G069.7−00.0 and PN G169.7−00.1 based only on our current H i measurements. For PN candidate PN G030.2−00.1, which was discussed by Anderson et al. (2011), its luminosity is ∼225 times stronger than the most luminous Galactic PN NGC 7027 (506 mJy at ∼8.6 GHz; see Zijlstra et al. 2008), so G030.2−00.1 might not be a PN.

In addition, our spectra have revealed that five of the PNs show larger tangent point velocities than expected from the rotation curve model when adopting an IAU value of $V_0 = 220\,\mathrm{km\,s^{-1}}$. Three of them are located near 53°. This is consistent with the previous studies in Levine et al. (2008) and Leahy et al. (2008).

We compare our distances with the previous measurements based on the data in Table 2 (also see Figure 20). We find that all other work (except statistical results; see Figure 20, left panel) show obvious dispersions among one another, and that our distance measurements are well consistent with the most reliable method, i.e., expansion parallax. Our distance measurements are consistent with Frew et al. (2016) when considering the uncertainties, but larger than the other statistical results (see Figure 20, middle and right panels). In order to investigate the possible effects of some PN parameters on our measurements, we have tried to find the correlation between these parameters (e.g., radius, reddening) and the residuals which were obtained by subtracting our distances from those obtained by other methods. No obvious correlation is found. A total number of 22 PNs have H i absorption measurements in the literature. Our work significantly increases the number of Galactic PNs with H i absorption measurements and known kinematic distances.

We acknowledge support from the NSFC (11473038, 11273025, 1126114046) and support from China's Ministry of Science and Technology under the State Key Development Program for Basic Research (2012CB821800, 2013CB837901). D.A. Leahy is supported by a grant from the Natural Sciences and Engineering Research Council of Canada. The work has made used of data from the International Galactic Plane Survey (http://www.ras.ucalgary.ca/IGPS/).

REFERENCES

Anantharamaiah, K. R., Radhakrishnan, V., & Shaver, P. A. 1984, A&A, 138, 131
Anderson, L. D., Bania, T. M., Balser, D. S., & Rood, R. T. 2011, ApJS, 194, 32
Bally, J., Pound, M. W., Stark, A. A., et al. 1989, ApJL, 338, L65
Bojičić, I. S., Parker, Q. A., Filipović, M. D., & Frew, D. J. 2011, MNRAS, 412, 223
Bovy, J., Allende Prieto, C., Beers, T. C., et al. 2012, ApJ, 759, 131
Cahn, J. H., Kaler, J. B., & Stanghellini, L. 1992, A&AS, 94, 399
Cazetta, J. O., & Maciel, W. J. 2000, RMxAA, 36, 3
Cazetta, J. O., & Maciel, W. J. 2001, Ap&SS, 277, 393
Ciardullo, R., Bond, H. E., Sipior, M. S., et al. 1999, AJ, 118, 488
Condon, J. J., & Kaplan, D. L. 1998, ApJS, 117, 361
Crovisier, J. 1978, A&A, 70, 43
Dickey, J. M., & Lockman, F. J. 1990, ARA&A, 28, 215
Dobbs, C. L., Bonnell, I. A., & Pringle, J. E. 2006, MNRAS, 371, 1663
Eisenhauer, F., Genzel, R., Alexander, T., et al. 2005, ApJ, 628, 246
Frew, D. J., Parker, Q. A., & Bojičić, I. S. 2016, MNRAS, 455, 1459
Gathier, R., Pottasch, S. R., & Goss, W. M. 1986a, A&A, 157, 191
Gathier, R., Pottasch, S. R., & Pel, J. W. 1986b, A&A, 157, 171
Giammanco, C., Sale, S. E., Corradi, R. L. M., et al. 2011, A&A, 525, A58
Gruendl, R. A., Chu, Y.-H., Guerrero, M. A., & Meixner, M. 2004, BAAS, 36, 138.05
Hajian, A. R., Terzian, Y., & Bignell, C. 1993, AJ, 106, 1965
Harris, H. C., Dahn, C. C., Canzian, B., et al. 2007, AJ, 133, 631
Heyer, M. H., & Terebey, S. 1998, ApJ, 502, 265
Jackson, J. M., Rathborne, J. M., Shah, R. Y., et al. 2006, ApJS, 163, 145

Jacoby, G. H., Morse, J. A., Fullton, L. K., Kwitter, K. B., & Henry, R. B. C. 1997, AJ, 114, 2611
Jones, D., Boffin, H. M. J., Miszalski, B., et al. 2014, A&A, 562, A89
Kaler, J. B., & Lutz, J. H. 1985, PASP, 97, 700
Kwitter, K. B., Méndez, R. H., Peña, M., et al. 2014, RMxAA, 50, 203
Leahy, D. A., & Tian, W. W. 2008, AJ, 135, 167
Leahy, D. A., & Tian, W. W. 2010, in ASP Conf. Ser. 438, The Dynamic Interstellar Medium: A Celebration of the Canadian Galactic Plane Survey, ed. R. Kothes, T. L. Landecker, & A. G. Willis (San Francisco, CA: ASP), 365
Leahy, D. A., Tian, W. W., & Wang, Q. D. 2008, AJ, 136, 1477
Levine, E. S., Heiles, C., & Blitz, L. 2008, ApJ, 679, 1288
Luo, S. G., Condon, J. J., & Yin, Q. F. 2005, ApJS, 159, 282
Maciel, W. J. 1984, A&AS, 55, 253
Masson, C. R. 1986, ApJL, 302, L27
Masson, C. R. 1989, ApJ, 336, 294
McClure-Griffiths, N. M., Dickey, J. M., Gaensler, B. M., et al. 2005, ApJS, 158, 178
Mellema, G. 2004, A&A, 416, 623
Mendez, R. H., Kudritzki, R. P., Herrero, A., Husfeld, D., & Groth, H. G. 1988, A&A, 190, 113
Morgan, D. H., Parker, Q. A., & Cohen, M. 2003, MNRAS, 346, 719
Napiwotzki, R., & Schoenberner, D. 1995, A&A, 301, 545
Navarro, S. G., Corradi, R. L. M., & Mampaso, A. 2012, in IAU Symp. 283, Planetary Nebulae: An Eye to the Future (Cambridge: Cambridge Univ. Press), 460
Phillips, J. P. 2004, MNRAS, 353, 589
Pottasch, S. R. 1983, in IAU Symp. 103, Planetary Nebulae, ed. D. R. Flower (Dordrecht: Reidel), 541
Pottasch, S. R., Goss, W. M., Gathier, R., & Arnal, E. M. 1982, A&A, 106, 229
Reid, M. J., Brunthaler, A., Menten, K. M., et al. 2007, in IAU Symp. 242, Astrophysical Masers and their Environments, ed. J. M. Chapman, & W. A. Baan (Cambridge: Cambridge Univ. Press), 348
Reid, M. J., Menten, K. M., Zheng, X. W., et al. 2009, ApJ, 700, 137
Shaver, P. A., Radhakrishnan, V., Anantharamaiah, K. R., et al. 1982, A&A, 106, 105
Stanghellini, L., Shaw, R. A., & Villaver, E. 2008, ApJ, 689, 194
Stil, J. M., Taylor, A. R., Dickey, J. M., et al. 2006, AJ, 132, 1158
Taylor, A. R., Gibson, S. J., Peracaula, M., et al. 2003, AJ, 125, 3145
Terzian, Y. 1997, in IAU Symp. 180, Planetary Nebulae, ed. H. J. Habing, & H. J. G. L. M. Lamers (Dordrecht: Kluwer Academic Publishers), 29
Tian, W. W., & Leahy, D. A. 2008, MNRAS, 391, 54
Tian, W. W., Leahy, D. A., Haverkorn, M., & Jiang, B. 2008, ApJL, 679, L85
Tian, W. W., Leahy, D. A., & Li, D. 2010, MNRAS, 404, 1
Tian, W. W., Leahy, D. A., & Wang, Q. D. 2007, A&A, 474, 541
van de Steene, G. C., & Zijlstra, A. A. 1995, A&A, 293, 541
Viironen, K., Greimel, R., Corradi, R. L. M., et al. 2009, A&A, 504, 291
Zhang, C. Y. 1993, ApJ, 410, 239
Zhang, C. Y. 1995, ApJS, 98, 659
Zhu, H., Tian, W. W., Torres, D. F., Pedaletti, G., & Su, H. Q. 2013, ApJ, 775, 95
Zijlstra, A., Pottasch, S., & Bignell, C. 1990, A&AS, 82, 273
Zijlstra, A. A., van Hoof, P. A. M., & Perley, R. A. 2008, ApJ, 681, 1296